

Review

Effect of Metal Atom in Zeolitic Imidazolate Frameworks (ZIF-8 & 67) for Removal of Dyes and Antibiotics from Wastewater: A Review

Zahra Pouramini ¹, Seyyed Mojtaba Mousavi ^{2,*}, Aziz Babapoor ³, Seyyed Alireza Hashemi ⁴, Chin Wei Lai ⁵, Yousef Mazaheri ⁶ and Wei-Hung Chiang ^{2,*}

¹ Department of Civil and Environmental Engineering, Tarbiat Modares University, Tehran 14117-13116, Iran

² Department of Chemical Engineering, National Taiwan University of Science and Technology, Taipei 10607, Taiwan

³ Department of Chemical Engineering, University of Mohaghegh Ardabili (UMA), Ardabil 56199-11367, Iran

⁴ Nanomaterials and Polymer Nanocomposites Laboratory, School of Engineering, University of British Columbia, Kelowna, BC V1V 1V7, Canada

⁵ Nanotechnology & Catalysis Research Center (NANOCAT), Institute for Advanced Studies, University of Malaya, Kuala Lumpur 50603, Malaysia

⁶ Department of Materials Science and Engineering, School of Engineering, Shiraz University, Shiraz 71946-84471, Iran

* Correspondence: mousavi.nano@gmail.com (S.M.M.); whchiang@mail.ntust.edu.tw (W.-H.C.)

Abstract: The use of antibiotics and dyes has resulted in severe water pollution and health risks; therefore, it is urgent to remove them from water sources. Among the most common methods for removing harmful water contaminants, adsorption and photodegradation are the most economical, simple, and reusable. Due to their high porosity, adjustability, and crystal structure, metal-organic frameworks (MOFs) are one of the effective adsorbents and photocatalysts. A typical MOF material is zeolitic imidazolate framework-8/67 (ZIF-8 and ZIF-67), comprising essentially of the metal atoms Zn and 2-methylimidazole (2-MIM). ZIF-8 and ZIF-67 have unique properties that make them efficient in water treatment due to high adsorption capacities and being good hosts for photocatalytic materials. In this article, a review study of the design and methods of synthesis of ZIF-8 and ZIF-67 composites is presented. An introduction to the current research on the role of ZIF-8 and ZIF-67 compounds as adsorbents and photocatalysts for wastewater pollution removal is provided. In this review study, we aim to supply a mechanistic perspective on the use of ZIF-8/67 composites in wastewater purification and present novel visions for the development of extremely effective ZIF-8/67-based adsorbents and photocatalysts. To unlock the full potential of ZIF-8/67 composites in dye and antibiotic removal and water recycling, current difficulties will be discussed in detail.

Keywords: zeolitic imidazolate framework-8/67; dyes removal; antibiotics degradation



Citation: Pouramini, Z.; Mousavi, S.M.; Babapoor, A.; Hashemi, S.A.; Lai, C.W.; Mazaheri, Y.; Chiang, W.-H. Effect of Metal Atom in Zeolitic Imidazolate Frameworks (ZIF-8 & 67) for Removal of Dyes and Antibiotics from Wastewater: A Review. *Catalysts* **2023**, *13*, 155. <https://doi.org/10.3390/catal13010155>

Academic Editors: Collin G. Joseph, Gianluca Li Puma, Giovanni Palmisano and Rubén Mas Ballesté

Received: 28 November 2022

Revised: 15 December 2022

Accepted: 3 January 2023

Published: 9 January 2023



Copyright: © 2023 by the authors. Licensee MDPI, Basel, Switzerland. This article is an open access article distributed under the terms and conditions of the Creative Commons Attribution (CC BY) license (<https://creativecommons.org/licenses/by/4.0/>).

1. Introduction

Water pollution seriously threatens human health and negatively affects the environment [1–3]. Therefore, the control and treatment of water pollution is very important and urgent. There are plenty of water pollution resources including different substances. Many emerging organic pollutants (EOCs) contaminate water supplies, which include drugs, cosmetics, and pollutants from industry such as dyes and pigments, etc. [4–6]. Even at low concentrations, most EOCs are more difficult to remove through water purification due to their physical and chemical features (e.g., highly water soluble) [7]. Dyes are utilized to impart color to materials for different purposes, involving art and protection. Dye and pigment are the two basic types of dyes. The compounds in the first group are organic and soluble. They impart permanent color to fabric and fiber surfaces and are resistant to light and detergents. Since dyes are soluble in water; they produce bright colors in acidic

environments [8–11]. However, pigments used in plastics, fibers, and polymeric materials are not soluble in the application medium [12]. After the dyeing process, dye-processing companies store their wastewater. The wastewater is then discharged into the environment and pollutes freshwater. Dye compounds are toxic, so it is not acceptable to discharge dyed wastewater into the environment without treatment [13]. It has been shown that oxygen dispersion and self-purification in water bodies are disturbed when colored wastewater is discharged into the environment [14–16]. Since the density of colored wastewater is lower than that of water, a visible layer of color forms on the water surface when colored wastewater is mixed with water sources. Because of the layer of color, sunlight cannot penetrate the water, preventing life from thriving under the surface, such as photosynthesis and respiration [17–19]. The commercialization and usage of antibiotics to treat bacterial infections has resulted in many public health advances. It is estimated that 90 percent of the active ingredients of antibiotics pass into urine and feces, thus entering the environment [20]. Pollution of water bodies by antibiotics is a worldwide concern. Overexposure to antibiotics leads to both health problems and resistance to antibiotics [21–25]. According to several studies, the urban water cycle contains antibiotics. This includes surface water, groundwater, drinking water, and wastewater [26–28], and domestic wastewater contains nearly 6 mg/L of lead [29,30]. Therefore, antibiotics must be removed from the natural aqueous environment using effective methods. There are various approaches for antibiotic removal, including biological treatment [31], electrochemical treatment [32], advanced oxidation technology [33,34], membrane filtration [35], adsorption [36], and photocatalytic degradation [37]. Generally, wastewater is treated via coagulation, filtration, and other techniques. Because of the high maintenance expenditures associated with these techniques, these approaches are not optimal [38]. Moreover, the conversion of pollutants into nontoxic substances is a major challenge. Treatment of pollutants via adsorption or photocatalysis can be more economical and energy efficient [39–43]. Researchers are exploring novel materials for the preparation of adsorbents and photocatalysts to achieve higher removal efficiency of pollutants [44–46]. Recently, a subclass of MOFs with zeolitic architecture as a hybrid framework has been synthesized for water purification. Among them, zeolitic imidazolate frameworks (ZIFs) have attracted a lot of consideration because of their exceptional features such as selective adsorption [47], capability to transfer electrons, ability to detect pollutants [48], biomedical applications [49], antibacterial applications [50], large functionalities [51], unimodal micropores, and stability chemically and thermally. ZIFs consist of a tetrahedral coordination of transition metal cations (Zn, Co) and an imidazolate linker [52–56]. There are numerous research papers in the literature on ZIFs, especially ZIF-8 and ZIF-67, which are used in the treatment of pollutants [57,58]. ZIF-8/ZIF-67 has a sodalite-like structure and consists of 2 MIM or Zn/Co ions. In their center, there is a micropore with a diameter of 11.6 Å, which is accessible through tiny openings with a diameter of 3.4 Å [59]. ZIF-8 and ZIF-67 have a very high surface area (1970 m² g) owing to the high porosity of the framework [60]. In addition, these substances possess stable chemical and thermal properties. For instance, ZIF-8 is able to maintain its framework under boiling water for about seven days, even at 100 °C for 24 h in an NaOH aqueous solution (up to 8 M) [61]; in general, the temperature of decomposition can reach 550 °C [60]. This review presents an overview of the studies and progress in the dyes and antibiotics removal from water using ZIF-67 and ZIF-8. In the following sections, we introduce ZIFs and discuss their role in water purification via adsorption, photocatalytic removal, and synthesis strategies. Using ZIF-8 and ZIF-67 composites for the adsorption or photocatalysis of pollutants in wastewater is illustrated by analysing some representative examples.

2. MOF

MOFs are porous hybrid materials containing organic and inorganic components, also known as absorbent coordination polymers. They have been extensively studied by scientists and engineers as a fascinating material [61]. They include inorganic metal ion secondary building blocks (SBUs), oxo-clusters, and bridging organic linkers. MOFs can

have different chemical compositions and shapes within certain structures, which offers the possibility of synergistic property combinations [62–65]. MOFs not only have large surface areas, ordered pore structures, crystallinity, and polymetallic sites, but also are compatible with polymers [66–68]. With their unique properties and structural diversity, MOFs are particularly attractive for removing toxic metals or EOCs from wastewater [69–72]. In contrast to traditional porous materials, MOFs possess a crystalline nature with a large surface area and ultrahigh porosity, mixed with an exceptionally high level of organic and inorganic composition, which enables them to be used for various applications, including membranes, catalysis, gas capture and storage, adsorption, and energy [73,74]. Each MOF family, including ZIF (zeolitic imidazolate framework), is distinguished by a different metal node or organic linker used in their synthesis. The water stability of any MOF is, however, a prerequisite for its use in aqueous solutions [67]. ZIF-8/67 subcategories of MOFs demonstrate this quality [52]. An overview of the general MOF synthesis pathway is shown in Figure 1.

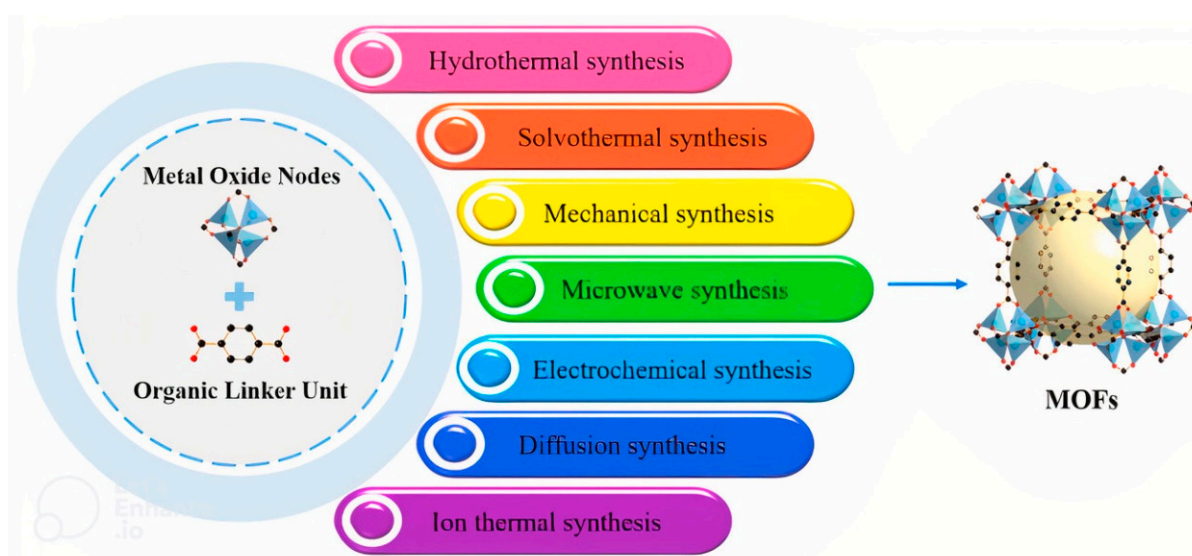


Figure 1. Synthesis pathway for MOFs, reproduced with permission from [75]. Copyright Elsevier, 2021.

ZIF materials contain a zeolite framework synthesized using metal sources such as Zn and Co and organic ligands such as imidazole or imidazole derivatives [76,77]. In addition to exhibiting MOF advantages in terms of structure, they also overcome their frailties like poor thermal and chemical stability [78,79]. In 1989, the Chen group synthesized ZIF-8 for the first time and named it MAF-4 [80]. Officially, it was named ZIF-8 after Yaghi's research group analyzed it systematically [52]. ZIF-8's chemical formula is $\text{Zn}(\text{Hmim})_2$, which is composed of 2 MIM and the metal atom Zn [59,81]. ZIF-8 offers a wider range of synthesis strategies compared to other MOF materials. Due to its robust bonding structure, ZIF-8 also exhibits higher chemical and hydrothermal stability. A great example of the thermal stability of ZIF-8 is its ability to maintain structural stability at temperatures equal to 500 °C. Moreover, ZIF-8 retains its porosity and crystallinity even after dissolution in water or organic solvents (Figure 2) [82–84]. Another important form of ZIFs is ZIF-67, which consists of cobalt cations (Co^{2+}) in combination with organic ligands such as 2-MIM. As a secondary moiety, the Co^{2+} group coordinates with a 2 MIM linker. The ZIF-67 has a cubic crystal structure of unit cell parameters $a = b = c = 16.95890$ [85]. In addition to separation, catalysis, water purification, adsorption [57], and carbon capture, ZIF-67 also has exceptional capabilities in other fields [54,86–88].

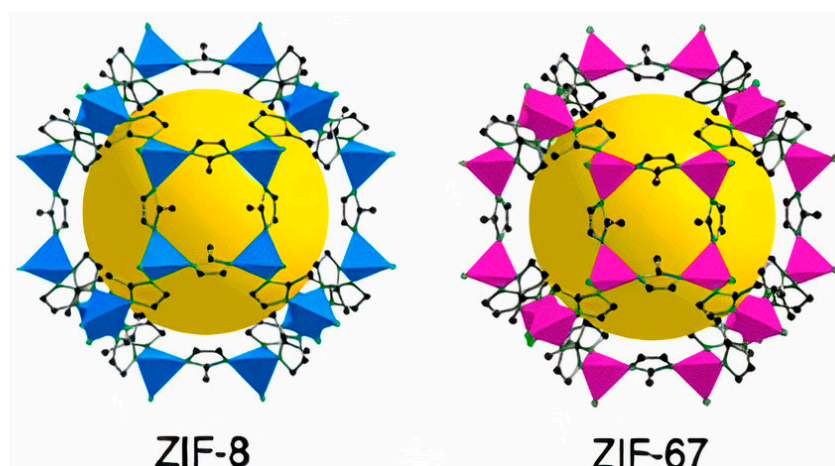


Figure 2. ZIF-8 and ZIF-67 structure, reproduced with permission from [58]. Copyright Elsevier, 2021.

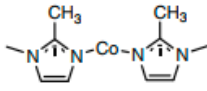
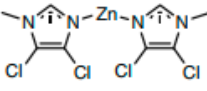
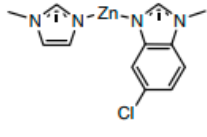
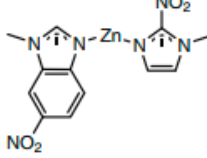
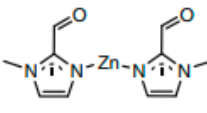
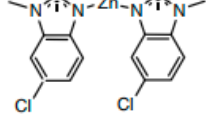
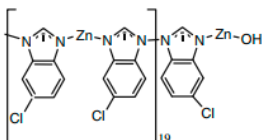
It is an efficient method to combine ZIF-67 with the other substances or structures, creating composites with better performance than ZIF-67 alone. Due to the excellent electrochemical, magnetic, and photoelectric properties of metal oxides and mixed metal oxides, these compounds are appealing because they have unique functional properties [89]. Derivatives of ZIF-67 metal oxide mix tailored ZIF-67 porosity with a large number of metal oxide framework functions. Several metal oxides for ZIF-67 were synthesized, and their performance was investigated as adsorbents, separators, catalysts, sensors, storage devices, and microwave-absorbing oxides (Figure 2) [90].

There are numerous active sites and facial charge separations on the surface of ZIF-8 and ZIF-67. Now, ZIF-8/67 materials are widely used in many forms including powders, colloid, and membranes or thin films and have been applied to a diverse range of important fields. New multifunctional composites/hybrids can be formed through the controllable integration of ZIF-8/67 and functional materials; these composites or hybrids exhibit more superior properties than individual components through the collective behavior of each functional unit and have attracted widespread attention [91,92]. To date, ZIF-8/67 composites have been successfully prepared with active species, such as fibers, metals, oxides, polyoxometalates (POMs), polymers, graphene, carbon nanotubes (CNTs), and so on. They can maintain the original properties and functions of each phase and also make up for the limitation of any single phase in application. Compared with pure microporous ZIF-8/67, ZIF-8 and ZIF/67 composite material not only enhances the adsorption capacity and photocatalytic activity of them, but also broadens the application range of ZIF-8 and ZIF/67 [44,93]. Table 1 describes some general properties of the ZIFs.

Table 1. Some general properties of the ZIFs.

ZIFs	Composition	Composition Structure	T/V ¹ (T/nm ³)	D _a ² (Å)	D _p ³ (Å)	Ref.
ZIF-8	Zn(MeIM) ₂		2.45	3.4	11.6	[94]
ZIF-9	Co(bIM) ₂		2.51	2.9	4.31	[94]
ZIF-10	Zn(IM) ₂		2.25	8.2	12.2	[82]

Table 1. Cont.

ZIFs	Composition	Composition Structure	T/V ¹ (T/nm ³)	D _a ² (Å)	D _p ³ (Å)	Ref.
ZIF-67	Co(MeIM) ₂		2.46	3.4	11.6	[82]
ZIF-71	Zn(dcIM) ₂		2.06	4.2	16.5	[82]
ZIF-76	Zn(IM)(cbIM)		1.03	1.9	1.9	[82]
ZIF-78	Zn(nbIM)(nIM)		2.08	3.8	7.1	[83]
ZIF-90	Zn(Ica) ₂		2.33	3.5	11.2	[95]
ZIF-95	Zn(cbIM) ₂		1.51	3.7	24	[96]
ZIF-100	Zn ₂₀ (cbIM) ₃₉ (OH)		1.29	3.4	35.6	[96]

¹ T/V is the density of metal atoms per unit volume, ² D_a is the diameter of the largest sphere that will pass through the pore, and ³ D_p is the diameter of the largest sphere that will fit into the cages without contacting the framework atoms. Pore metrics measurements exclude guests.

3. Methods of Synthesizing Materials Based on ZIF-67

3.1. Solvothermal

This approach is a commonly utilized method in ZIF-67 synthesizing. After the reactants such as sources of cobalt and 2-MIM (Hmim) are dissolved in the solvents, the solution is usually placed in the autoclave at 50 to 200 °C (Figure 3). Then, after 12 to 72 h, the crystals gradually form. Moreover, three important operations are involved in the solvothermal process, i.e., hydrolysis, coordination, and deprotonation, which control the properties of the material [97]. Jayashree et al. investigated the preparation of ZIF-67 materials using Co(NO₃)₂·6H₂O and Hmim in dimethylformamide (DMF) and CH₃OH, respectively, for four hours at 60 °C. According to the adsorption-desorption tests of N₂ and scanning electron microscopy (SEM), the solvent was the most important factor in the preparation of ZIF-67 crystals. When methanol and DMF were used as solvents, the synthesized ZIF-67 exhibited a microporous and hierarchical structure [98]. Because of the environmental pollution and high energy consumption in the conventional synthesis method, the use of new approaches in ZIF synthesis is beneficial to the environment. For example, using water as a solvent is one of the most environmentally friendly syntheses of ZIFs [99,100]. Zhang et al. reported a new zeolite-imidazole salt scaffold (ZIF-L-Co), which

is the transition phase of ZIF-67, formed by mixing $\text{Co}(\text{NO}_3)_2$ with Hmim in the aqueous medium. Reactant concentration and the molar ratios affected the handleable phase and samples morphology. When the Hmim/ Co^{2+} molar ratio is increased, the morphology changes from leaf-like sheets to rod-like frames. The irregular polyhedron smooths out with increasing size, and eventually visible edges and corners appear. In general, using water as a solvent accelerated the conversion of the ZIF-L-Co phase into ZIF-67 [101].

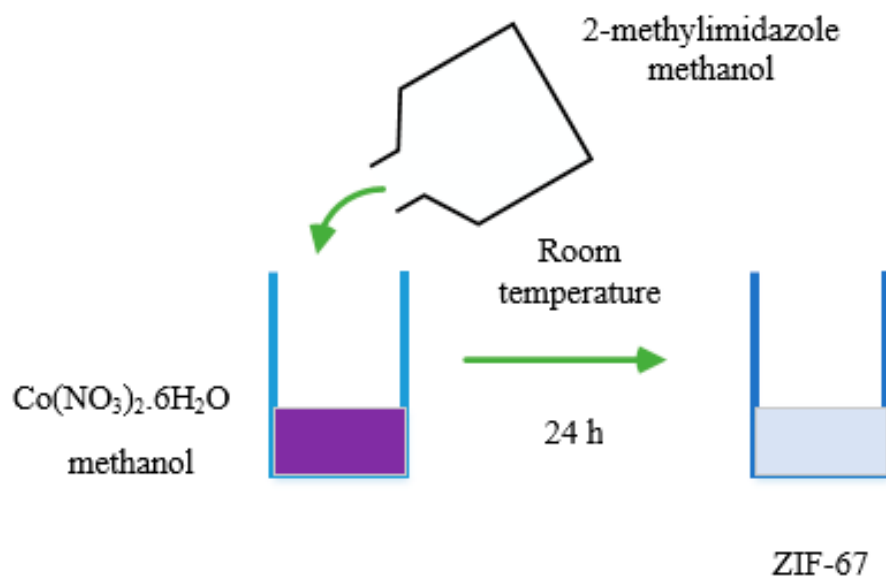


Figure 3. Synthesis process of solvothermal methods.

3.2. Surfactant-Assisted

In this process, the dissolution and dispersion of the product particles are improved by adding surfactants to the precursor solution [102,103]. The type and amount of surfactant chosen affect the structure and morphology of the sample [104]. For example, by mixing a cobalt source via an aqueous Hmim solution including cetyltrimethylammonium bromide (CTAB), ZIF-67 can be synthesized rapidly (about 5 min). During crystal formation, CTAB acts as a capping agent to modulate the particles size by 50–320 nm [105]. Li et al. investigated Fe_2O_3 @-ZIF-67 composite synthesis. After immersing Fe_2O_3 nanorods in DMF, polyvinylpyrrolidone (PVP), Hmim, and $\text{Co}(\text{NO}_3)_2 \cdot 6\text{H}_2\text{O}$ were added. The manufactured product was dried at 80 °C for 12 h. In this reaction, the PVP had the role of adjusting the size of the product and increasing the affinity of ZIF-67 and Fe_2O_3 [106].

3.3. Sol–Gel

The technology of sol-gel has proven to be a practical way for controlling the mixing and frameworks of molecules at different length scales [107]. Generally, a suspension of colloidal with submicron particles is obtained from MOF precursors in collaboration with coagulants via condensation and hydrolysis processes. Subsequently, solid particles are formed over the gels due to the spatial structure during heat treatment [108]. Xu et al. fabricated an aerogel from Fe_3O_4 /ZIF-67@WA (WA = wood aerogel) by incorporating magnetic Fe_3O_4 /ZIF-67 materials into a natural lightweight WA in situ. First, Fe_3O_4 nanoparticles (NPs) were purified with a Co_2p -containing PVP solution. Then, the Co_2p -containing PVP solution and Fe_3O_4 NPs were anchored on a wood aerogel laminate surface. Due to the oxygen groups in the extended cellulose chain, the existence of Hmim, and the strong hydrogen bonding, crystals of ZIF-67 grew on the wood aerogel (Figure 4) [109].

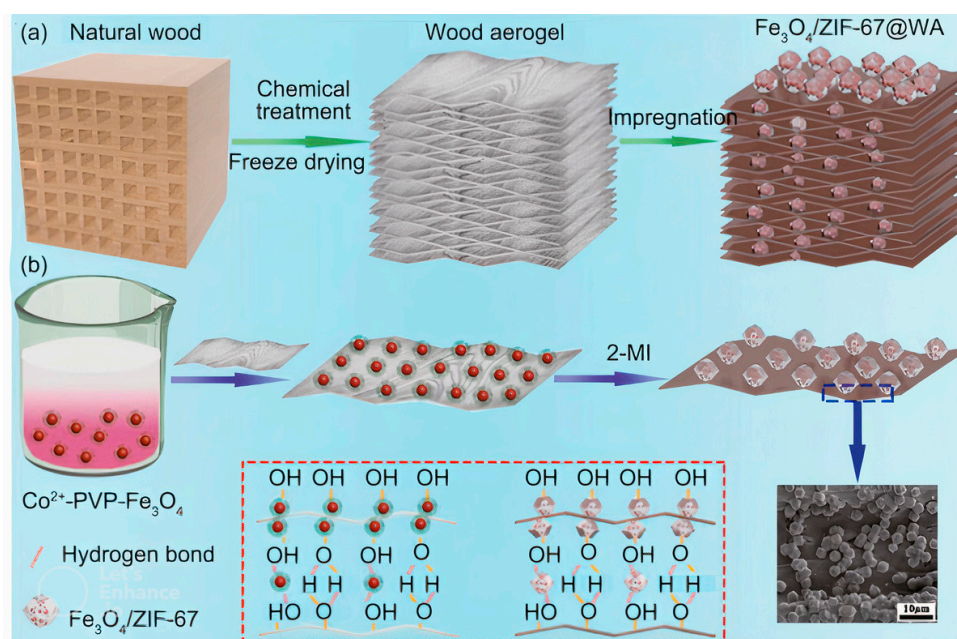


Figure 4. Process of Fe₃O₄/ZIF-67@WA aerogel preparation (a) Converting natural wood to Fe₃O₄/ZIF-67@WA; (b) Final properties of Fe₃O₄/ZIF-67@WA, reproduced with permission from [109]. Copyright Elsevier, 2019.

3.4. Microwave/Ultrasound-Assisted

Recently, the production of ZIF-67 using microwave and ultrasonic methods has attracted much interest. The generation of heat and pressure can facilitate the introduction of small particles and increase the purity of the phase in a short reaction time [110,111]. Niyaz et al. examined the synthesis of ZIF-67@Fe₃O₄@ESM (ESM = eggshell membrane) composite using ultrasound-assisted technology. According to them, the Co(NO₃)₂ solution was sonicated, combined via Fe₃O₄@ESM in the water phase, and sonicated again in the Hmim solution until the crystals of ZIF-67 grew. Using the prepared adsorbents, copper cation (Cu²⁺) capture and dye (Basic Red 18: BR18) adsorption processes have been designed and thoroughly studied. In experiments conducted with the ZIF-67@Fe₃O₄@ESM composite, it has been found that the adsorption rate and removal percentage for both types of contaminants are faster and higher than that of pure ZIF-67 when compared with the composite (Figure 5) [112].

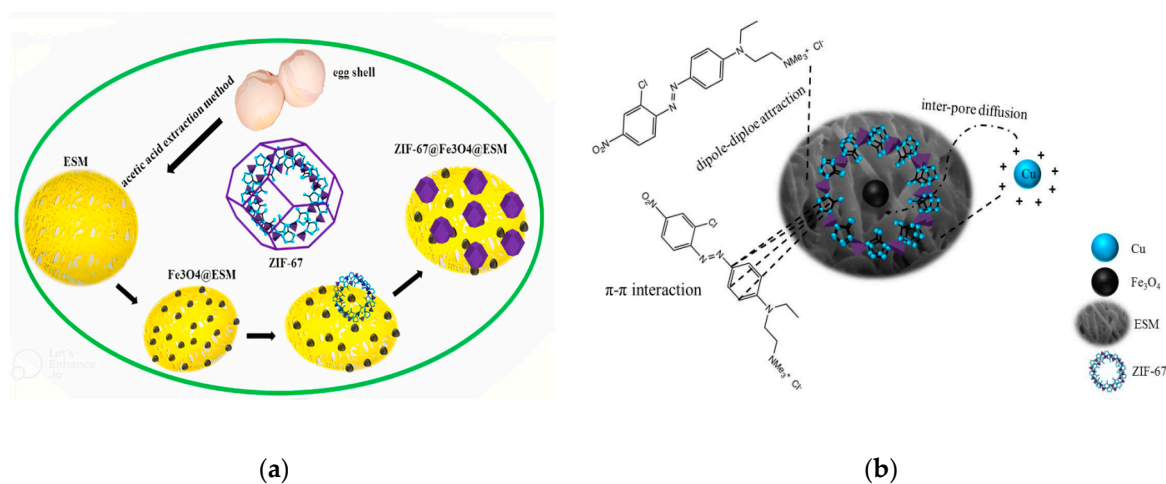


Figure 5. (a) Green synthesis of ZIF-67 @Fe₃O₄@ESM; (b) adsorption mechanism, reproduced with permission from [112]. Copyright Elsevier, 2019.

4. Methods of Synthesizing Materials Based on ZIF-8

4.1. *In Situ*

The in-situ process is a straightforward approach. However, it requires special conditions for the properties of the materials. In this method, some unique functional groups and surface properties of the elemental substances should be used to propagate the interactions and biochemical reactions and achieve binding without modifying them [113]. Lee and Hwang et al. studied the fabrication of PS @ZIF-8 core-shell particles. Polystyrene microspheres (PS) are utilized as supports and then successively integrated by ZIF-8 via the groups of hydroxyl linking the PS microspheres to ZIF-8. Modification of the nuclei via a negative charge for adsorbing Zn^{2+} causes ZIF-8 to grow near the nuclei. ZIF-8 shell thickness can be modified through growth cycle control [114].

4.2. *Modifying Surfaces*

In the modifying surfaces method, the core particles surface is treated using coupling agents, surfactants, and crystal nuclei to enhance the binding and adsorption strength among ZIF-8 and the NPs and to achieve a close mixture between them. The ease of use and good applicability are two major advantages of this approach [115,116]. Lu et al. investigated the encapsulation of various inorganic NPs in ZIF-8 using PVP to functionalize the NPs. First, they succeeded in encapsulating functional guests in situ in ZIF-8 crystals [91]. Then, they succeeded in encapsulating most of the nanoparticles, rods, and spheres. To enhance the mixture of NPs and ZIF-8 materials, two nonpolar denominators were combined with an organic ligand. The secondary seed crystal growth method is a kind of surface modification technology; nanoscale seed particles of ZIF-8 are used as an alternative method of loading and modifying carrier particles using chemical reagents, and the growth of the ZIF-8 crystals is accelerated under the influence of the lead structure of seed crystals. Finally, a continuous and dense shell of ZIF-8 is generated around the carrier. The modifying surfaces method reduces ZIF-8 crystals' sensitivity to environmental factors of synthesis and crystallization from solution [44].

4.3. *Template Synthesis*

This approach is classified into two groups: the process of soft template (using some molecular systems) and the method of hard template (some materials with rigid structure), in which threshold limitations affect the growth of the shells and the size of the nuclear particles at a given location. Surfactants and ions are generally utilized for stabilizing the pre-synthesized NPs and caps. In the next step, the NPs are placed in a solution containing ZIF-8 molecular structure blocks, and ZIF-8 is applied to the NPs. In research, comparing ZIF-8 to conventional porous materials like zeolites, ZIF-8 is an effective host for guest materials because the modifiable pores and high porosity of ZIF-8 allow rapid access to entrap particles and accelerate mass transfer [117,118]. The microemulsion approach is counted among the soft template process. The fundamental is based on the formation of an emulsion using two incongruent solvents under the surfactants action; the reactants nucleate in the center of the microbubbles or on the outer wall and then fuse to make core-shell particles that are monodisperse or monodisperse hollow due to excellent interfacial properties [44].

5. Advantages and Disadvantages of ZIF8/67

Due to their zeolitic topology, high flexibility and multifunctional properties are potential advantages of ZIFs. The fine dispersion and better absorptivity of ZIFs make them excellent candidates for electrochemical sensing. Even when organic solvents reflux, alkaline solutions are present, and water is present, ZIFs show consistent performance in gas adsorption [119]. Among ZIF shapes, ZIF-67 is closely related to a cage-like shape and essential for hollow and core-shell structures. This structure facilitates mass transfer, prevents dissolution, and shortens the time required for ions to disperse. This makes ZIF one of the most important starting materials for super capacitor electrodes [120]. Several heterogeneous catalytic reactions are carried out with ZIF-67-based materials, including

redox reactions, addition reactions, esterification, hydrogenation, and hydrogenation-dehydrogenation [100]. With a degree of inhibition of 81%, the epoxy-coated cobalt-based nanoporous ZIF-67 showed good corrosion protection properties [121]. Synthesized ZIF-8 nanostructures with a high surface area, good porosity distribution, and bimetallic ions were characterized by their solvothermal properties. In the detection of nitrogen dioxide, ZIF-8 nanostructures are highly selective and responsive sensors [122]. Another major advantage of ZIF-8/67 is their ability to change the pore size and structure as efficiently as possible. In addition, the conventional microporous ZIF-8 has been greatly enhanced by the mesoporous development and multilayer porous ZIF-8. There are many active sites on ZIF-8 surface, as well as a separation of facial charges. There are several important applications for ZIF-8 materials, involving powders, colloid materials, membranes, and thin films [83]. The surface area of porous materials is the main criterion for determining their porous nature. ZIFs have a large surface area, which can be determined by measuring Brunauer–Emmett–Teller (BET). Partial or low activation of the samples can sometimes lead to low surface area [123]. Nitrogen adsorption/desorption, Langmuir, and BET analyses are performed for evaluation [124]. In general, ZIF-8 NPs possess a special surface area of 1500–2500 m² g⁻¹, a higher surface area than most other adsorbents. By combining functional materials, ZIF-8 composites achieve better stability in water, ability to recycle, and higher porosity and pore size [44,125]. ZIF-67 possesses a large surface area (about 1700 m² g⁻¹) providing large active sites, and the macropores (pore diameter of about 0.340 nm) are advantageous for reactions owing to their guest molecule attachment [126,127]. The cost of ZIFs is always the biggest problem for industrial production and large-scale applications. Solvothermal synthesis of ZIFs usually uses organic solvents such as CH₃OH, DMF, and NMP for production and input of energy throughout synthesis. Up to 70% of the production cost of ZIFs is due to high-cost precursor substances, such as metal salts and organic ligands and solvents [128]. To save costs, environmentally friendly and simple methods for the production of ZIFs are essential. For instance, using a hydrothermal process rather than a solvothermal process for preparing ZIFs is an effective way to avoid hazardous organic solvents. Furthermore, some ZIFs are produced without the use of electricity at room temperature. In recent years, ZIFs have been synthesized using dry gels and mechanochemical processes, reducing organic ligand use or solvents and offering commercial potential [129]. To make ZIF-based materials a more efficient, novel method for inexpensive synthesis, we need to know more about the crystallization mechanism of ZIF. Chemical waste recovery can further reduce production costs through continuous synthesis processes [130,131]. Secondary pollution of the environment may result from ZIFs entering water during wastewater treatment. ZIFs have stability problems that can cause them to naturally enter water. A ZIF surface formed from the chemical combination of zinc ions, cobalt ions, and imidazole is relatively hydrophobic and insoluble in water. In addition, in recent research, it has been observed that soaking ZIFs in water causes them to lose their central metal ions [132,133], and the hydrolysis or deformation of ZIFs in water has now been confirmed by several researchers [134–136]. To prevent ZIFs from collapsing due to attacks on the metal coordination bonds, their stability must be improved. The use of ZIF powder may lead to clogging of the pipelines and loss of adsorbents during treatment. The importance of separating the spent ZIFs from the treatment chambers quickly and efficiently cannot be overstated. Several solutions are currently being aimed at assuring adequate contact of contaminants with ZIFs and safe reuse of ZIFs. These include bonding ZIFs with effortlessly reusable magnetic materials, mixing ZIFs with filter membranes, and applying ZIFs to macrosubstrates [92,112,137–141].

6. Application of ZIFs in Removing Pollutants from Wastewater

ZIFs have excellent properties that allow them to be utilized as adsorbents and photocatalysts to efficiently eliminate various wastewater pollutions. The potential for their application in wastewater regeneration is immeasurable. The adsorption process is effective methods of wastewater treatment owing to its simplicity, cost efficiency, and lack of

unwanted byproducts. A necessary component of the adsorption process is the research of highly effective sorbents. Therefore, it is ideal to enhance the adsorption capability of a particular adsorbent by improving its structure and morphology [44]. Due to its revolving door effect, ZIF-8 is able to adsorb large molecules exceeding its pore size. Yaghi's experiments have also shown that ZIF-8 can be easily modified and synthesized so that it can be mixed with other materials to form a highly effective adsorbent [52]. Unlike conventional adsorbents, composites of ZIF-8 are able to reduce the adsorbents aggregation, and the adsorbent can be separated from water more efficiently. In the removal of water contaminants, ZIF-8 composites show better adsorption capacity and recyclability than individual components [45,142]. For adsorption applications, an excellent level of stiffness and robustness is required for ZIFs to maintain their structural stability under high pressure. The structure of the pores is determined by acid-base interactions, electrostatic interactions, π -bonds, stacking, coordination interactions, and hydrogen bonding [76]. In this way, molecules that fit perfectly into the pores are preferentially adsorbed, while molecules that are too big or too tiny are excluded [143]. One of the current methods for treating water pollutants is catalytic oxidation, which includes photocatalytic oxidation, catalytic Fenton oxidation, ozone oxidation, and electrochemical catalysis. Photocatalysis is characterized by consuming little energy under mild circumstances, which makes it an ideal method for reducing organic pollutants and other harmful contaminants [144,145]. A photocatalytic process is capable of degrading organic pollutants more efficiently than adsorption. In the decomposition of mental iron, photocatalysis usually produces undesirable byproducts. It can, however, effectively remove many organic pollutants from water by converting them to carbon dioxide and water, and inorganic contaminants can be converted to harmless compounds via oxidation and reduction. Currently available photocatalysts have two main problems: their low quantum yield and poor conversion of solar energy limiting their application in wastewater purification [146]. The advancement of photocatalysts with increased activity and low cost, especially photocatalysts that respond to visible light, would considerably improve the efficacy of using sunlight. Semiconductor materials are frequently utilized as photocatalysts because of their great efficacy in converting solar energy. Since TiO_2 has a wide photosensitivity bandwidth and is suitable for UV radiation, it is widely used as a photocatalyst [147]. CdS , ZnO , WO_3 , and ZnS are also synthesized as semiconductors with photocatalytic activity. Photocatalytic degradation materials have the potential to be used for pollution control, but most of them require ultraviolet light irradiation to degrade pollutants, and the solar energy utilization is generally insufficient. It is possible to develop novel photocatalytic materials by using composites based on MOFs. Table 2 compares the efficiency of ZIFs with some other catalysts. The organic functional groups in ZIF-8 have the potential to exhibit catalytic activity, and the wide pore volume makes it suitable for use as a catalyst. For ZIF-8 to be used as a catalyst, catalytically active particles must be combined to promote bulk diffusion. At the same time, the porous structure acts as a molecular separator to achieve selective catalysis. Once ZIF-8 with semiconductor properties is exposed to UV light, electrons and holes are generated, which is the first reaction step of photocatalysis. Because of the large band gap of ZIF-8 (4.90–5.10 eV) and insufficient electron release capability, its photocatalysis performance is generally worse than that of conventional semiconductors. Different procedures have been used to decrease the band gap and improve the efficiency of electron discharge. For example, ZIF-8 has been combined with metal oxides or various linkers or metal centers have been used to improve the photocatalytic activity [148,149]. ZIF-67 derivatives can also be used as photocatalysts. There are two crucial components for this process: transition metal cations (Co) and active organic ligands (imidazolates), which exhibit charge separation properties and broad visible absorbing, catalytic properties, adjustable pore size configurations, and chemical and thermal stability. According to Park et al., ZIF-67 exhibits photocatalytic abilities under the conditions of the entire light spectrum. Consequently, it was found that it can contribute to the study of effective photocatalytic reactions capable of capturing and utilizing the entire light spectrum [150].

Table 2. A comparison of dye and antibiotic removal efficiency using different catalysts.

Catalyst	Pollutant	Operating Conditions	Findings	Ref.
Fe ₂ O ₃ -TiO ₂	Methyl blue	[Catalyst] = 0.4 g [MB] = 1 × 10 ⁻⁵ mol/L	Maximum MB degradation was obtained using 5 wt.% Fe-TiO ₂ @ 600 °C. Degradation efficiencies of 87%, 78.5%, and 69.2% were achieved for the first, second, and third cycles, respectively.	[151]
Fe ³⁺ -TiO ₂	Acid orange (AO7)	[Catalyst] = 25–300 mg/L [AO7] = 50 mg/L pH = 3, 5, and 9 [H ₂ O ₂] = 15 mg/L [air, k] = 2.49 h ⁻¹ [NaCl, k] = 2.54 h ⁻¹	UV-light: complete degradation and 91% mineralization was obtained in 2.5 h using 3 wt.% Fe ³⁺ TiO ₂ Visible light: complete degradation and 92.8% mineralization was obtained in 7 h using 2 wt.% Fe ³⁺ TiO ₂ . The photocatalytic system exhibited photochemical stability for at least 6 runs with degradation loss <9%.	[152]
P-Fe ₂ O ₃ -TiO ₂	Sulfamethoxazole (SMTZ)	[SMTZ] = 10 mg/L	Complete degradation of SMTZ and 30% mineralization were obtained under optimum conditions of P doping (1.2 wt.%), solution pH (3), and catalyst dosage (1.25 g/L). SMTZ degradation efficiency remained stable up to three cycles.	[153]
WO ₃ /SiO ₂	Methyl blue and imidacloprid (ICD)	[Imidacloprid] = 5 mg/L [MB] = 10 mg/L pH 7.5 Light source: 65 W lamp, λ > 420 nm, 125 W/m ² .	Degradation of ICD and MB was obtained 59% and 91% in 60 min and 120 min, respectively.	[154]
Ag/AgCl@ZIF-8/gC ₃ N ₄	Levofloxacin	Mass ratio of Ag/AgCl@ZIF-8 to g-C ₃ N ₄ = 10%, 87.3%	LVFX was degraded 94.5% within 60 min in the presence of 2.0 mM PMS.	[155]
ZIF-8/Fe ₂ O ₃	Reactive Red 198	ZIF-8/Fe ₂ O ₃ composite nanofibers (ZFCN) with different amounts of Fe ₂ O ₃ nanofiber (5, 10, and 20%).	ZFCN showed the highest dye degradation and removed Reactive Red 198 (RR198) at almost 94%.	[156]

6.1. Adsorptive Dye and Antibiotic Removal from Wastewater by ZIF-8 and ZIF-67

Organic pollutants are more common in wastewater than inorganic pollutants, such as organic dyes, organic pollutants that are particularly harmful to the environment, and pharmaceuticals and personal care products (PPCPs). Dye wastewaters are one of the complex wastewaters, both domestically and internationally, because of their high chemical oxygen demand (COD), biochemical oxygen demand (BOD), and refractory properties. Organic dyes not only enhance the hue of water, but also affect the appearance of water. In addition, the water is prevented from absorbing sunlight and there is a reduction in dissolved oxygen. Aquatic organisms suffer from these effects, and even the whole ecosystem of the waterbody may be destroyed, so proper management is required [157,158]. Anionic MO dyes, cationic rhodamine B (RhB) dyes, malachite green (MG), methylene blue (MB) dyes, etc. are common persistent dyes [159,160]. The decomposition of organic contaminants is complex, and their residues are easily visible in water. Most PPCPs are present in wastewater at low concentrations, including pharmaceuticals, fragrances, cosmetics, sunscreens, hair dyes, and other substances [161]. It has been reported that various composites of ZIF-8 can eliminate dyes from water, e.g., Fe₃O₄@ZIF-8, ZIF-8/PC-SMM, TiO₂@ZIF-8, etc. [162,163]. Dai et al. used an aqueous solution of MG to evaluate the function of a newly formulated ZIF-8 [164,165]. In this research, ZIF-8 grew uniformly

on the surface of supermacroporous polyacrylate carboxyl microspheres (PC-SMM) and made ZIF-8/PC-SMM composites. In addition to the adsorption properties of ZIF-8, the prepared ZIF-8/PC-SMM had a spherical shape so that the NPs of ZIF-8 came into contact with the molecules of MG. The ZIF-8/PC-SMM composites had a 128-fold larger specific surface area than the PC-SMM microspheres, based on the characterization of BET. Since MG could not penetrate the ZIF-8 pores and reach the inner part of PC-SMM, most of the MG adsorption occurred at the surface of ZIF-8. The charging effect could lead MG to be adsorbed by ZIF-8, while the imidazole rings could bind to the MG benzene rings. The results of the last experiment show that ZIF-8/PC-SMM adsorption capacity reached 101.20 mg g^{-1} , which was more than that of pure ZIF-8 and the commonly used resin materials. Moreover, the recovered composites of ZIF-8/PC-SMM successfully retained 98.8% of their original MG adsorption capability after three recycling cycles. Currently, dye degradation can also be achieved with enzyme-based ZIF-8 materials [166]. Yu et al. coated Fe_3O_4 @ZIF-8 particles with laccase and prepared Fe_3O_4 @ZIF-8-Lac composites for dye adsorption (Figure 6) [163]. Immobilization of laccase eliminated the volatility of free laccase and limited recycling. Fe_3O_4 @ZIF-8-Lac showed higher thermal stability and longer storing stability and activity than laccase alone in thermal tests. In addition, Fe_3O_4 @ZIF-8-Lac showed good performance in multiple dye degradation processes.

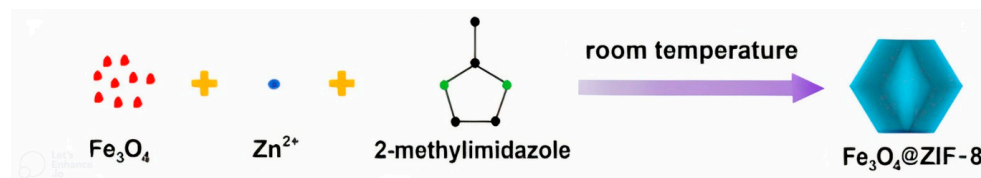


Figure 6. Process of Fe_3O_4 @ZIF-8 synthesis, reproduced with permission from [163]. Copyright Elsevier, 2019.

ZIF-67 showed excellent adsorption abilities to remove various harmful impurities such as Cr (VI), benzotriazole, methyl orange (MO), MG, phenol, and 1-naphthol. The high absorption of ZIF-67 for organic compounds is attributed to its surface structure, affinity for Co cations, hydrophobic pores, coordination of unsaturated points, and higher durability. However, the separation of ZIF-67 from wastewater is extremely energy intensive as it requires a very high centrifugation speed. A hybrid material of Fe_3O_4 and ZIF-67 was developed as a solution to the problem. Yang et al. synthesized Fe_3O_4 -PSS/ZIF-67 (PSS = polystyrenesulfonic acid) with a core-shell structure, named MZIF-67. The shell morphology can be attributed to polystyrenesulfonate (PSS), which has the functional group $-\text{SO}_3^-$. In addition to their biocompatibility, these composites exhibited excellent selectivity and magnetic features, so that they are effortlessly separated from wastewater with an external magnetic field. In addition, MZIF-67 showed rapid adsorption during the first seven hours of contact, and then a slow rate of adsorption, indicating that equilibrium can be reached after 24 h of contact. To examine the magnetic features of MZIF-67, MO removal from the MO/MB solution was also examined. Before and after magnetic separation, UV-Vis spectra of the MB/MO mixed solution were observed with a separation efficiency of 96%, where the MO anions were bound to MZIF-67 and the MB cations remained in the solution [88]. Li et al. reported a microporous Fe_3O_4 /ZIF-67 with a rhombic dodecahedral structure, which has a specific surface area of $528.90 \text{ m}^2 \text{ g}^{-1}$, a pore size dispersion of 0.65–1 nm, and a pore volume of $0.26 \text{ cm}^3/\text{g}$. The synthesis of Fe_3O_4 /ZIF-67 followed the same method as Yang, but PSS was omitted. As a result, ZIF-67 formed a uniform dodecahedral structure to which spherical Fe_3O_4 particles were attached [167,168]. This composite was used in the removal of blue 80 (DB80, azo dye) directly from water. In addition, the impact of various factors such as contact time, adsorbent dose, temperature, pH, and initial concentration on the adsorption capacity was analyzed. The outcomes show that the adsorbent Fe_3O_4 can be easily separated due to its magnetic properties. A magnetization saturation of 6.620 emu g^{-1} was found in the sample, indicating a paramagnetic character.

As a result, $\text{Fe}_3\text{O}_4/\text{ZIF-67}$ can be easily separated using an external magnetic field [169]. A composite of bio-based magnetic particles based on ZIF-67 ($\text{ZIF-67}/\text{Fe}_3\text{O}_4/\text{ESM}$) was synthesized by Mahmoodi et al. to study the heavy metals (Cu^{2+}) adsorption and removal of dyes. In this study, ESM was used as a low-cost, environmentally friendly polymer and magnetized to improve adsorption. An analysis of the effects of various operating parameters on $\text{ZIF-67}/\text{Fe}_3\text{O}_4/\text{ESM}$ adsorption was performed, and optimal circumstances for the procedure were selected: $\text{pH} = 5$, room temperature, Cu^{2+} concentration = 15 mg/L, and adsorbent dosage = 0.006 g [112]. Among the PPCPs, ciprofloxacin (CIP) is a representative compound. The compound is stable in terms of its chemical properties and stays in a natural condition for a long time because of its antibacterial properties. Yuan et al. investigated the use of konjac glucomannan (KGM)-based aerogels immobilized with ZIF-8 particles to CIP adsorption. The KGM/ZIF-8 composites consisted of 3D open-pore structures [146]. KGM was a cost-effective and biodegradable material that could be converted into aerogels with a high specific surface area via facial deacetylation [144]. The combination of ZIF-8 with KGM-based aerogels resulted in a more positive charge, and KGM/ZIF-8 could adsorb most of the CIP via electrostatic interactions. The combination of ZIF-8 with KGM-based aerogels resulted in a more positive charge, and KGM/ZIF-8 was able to adsorb most of the CIP via electrostatic interactions. A ZIF-8 composite fiber, PDA, and PAN was synthesized with electrospinning and utilized by the Chao group to adsorb tetracycline (TC) [69]. Due to its flexible and durable properties, polyacrylonitrile (PAN) has always been used as a template for electrospinning fibers. By incorporating PDA into PAN fibers, the hydrophilicity of PAN was improved, and ZIF-8 was loaded onto PAN fibers. The ZIF-8/PDA/PAN adsorption process on TC was analyzed by Chao et al. using the model of Weber–Morris. They concluded that intraparticle diffusion and surface adsorption have a crucial role in the adsorption procedure. The surface functional groups of ZIF-8 mainly adsorb TC; the open metal Zn adsorbs TC via coordination interactions because Zn and oxygen form strong chemical bonds. TC can also be removed by p-p stacking interactions between imidazole rings of ZIF-8 because they can act as aromatic molecules. The ZIF-8/PDA/PAN adsorption efficacy was compared to the ability of single functional materials after five cycles and achieved above 85% of the primary capacity. Chen et al. (2019) developed a simple one-point method to prepare hierarchical porous ZIF-8 (HpZIF-8) to remove TC and CAP. Polydiallyldimethylammonium chloride (PDAA) was used as a patterning agent to regulate the growth of microporous ZIF-8. Despite a smaller BET surface area, the modified material had a larger adsorption capacity than microporous ZIF-8 prepared under reflux heat [170]. It was successfully demonstrated that CIP could be eliminated from the aqueous phase by utilizing a nanoporous carbon (NPC) derived from the carbonization of ZIF-8 at 700 °C (NPC-700). CIP had the highest sorption capacity (416 mg/g) compared to other adsorbents. The material could be reused up to seven times [171]. The effectiveness of ZIF-8 in removing a mixture of TC and oxytetracycline hydrochloride (OTC) was investigated. ZIF-8 simultaneously removed 90.7% of TC and 82.5% of OTC in batch experiments. Both TC and OTC had a maximal adsorption capability of 303.0 and 312.5 mg/g, separately. The TC and OTC adsorption at 303 K, TC, and OTC had pseudo-second order kinetics that best fit the Langmuir adsorption model with $R^2 = 0.9630$ and 0.9810 , respectively. ZIF-8 had a high specific surface area ($1158.20 \text{ m}^2 \text{ g}^{-1}$), and SEM and transmission electron microscopy (TEM) showed that antibiotics were adsorbed on its surface. ZIF-8, after reaction via X-ray powder diffraction and Fourier transform infrared spectroscopy, showed benzene ring structures on its surface associated with both contaminants, confirming adsorption. ZIF-8 also exhibited C=O double bonds on its surface, suggesting the presence of antibiotics. It is likely that the mechanism causing adsorption involves the presence of π - π interactions among the coupled groups in TC/OTC and the ZIF-8 imidazole rings [172]. Ahmadi et al. investigated ZnO@ZIF-67 , containing various concentrations of ZnO (0.03, 0.05, and 0.09 g) and named as ZnOZ (0.03), ZnOZ (0.05), and ZnOZ (0.09), respectively. The synthesis of ZIF-67 and ZnOZ composites was carried out at room temperature. FTIR, SEM-, EDX, XRD, and BET analyses were performed on the synthetic materials ZIF-67, ZnO, ZnOZ

(0.03), ZnOZ (0.05), and ZnOZ (0.09) to remove TC from water. Various parameters of the aqueous medium were also investigated, involving pH, initial concentration of pollution, dose of adsorbent, contact time, and temperature. TCC was removed using pseudo-second order kinetics and the Langmuir isotherm. Moreover, thermodynamic data confirmed that adsorption of TCC was spontaneous and endothermic. The ZnO@ZIF-67 nanocomposite was a good adsorbent for the removal of pharmaceutical impurities from aqueous media [173]. Another study showed that an adsorption composite material, ZIF-67@WA, could be prepared by anchoring rhombic ZIF-67 dodecahedra in wood aerogel synthesized via selective lignin and hemicellulose removal from wood. The lamellar structure of WA creates suitable attachment sites for ZIF-67, and 32.65 wt% ZIF-67 was present in the composite. The crystallinity of ZIF-67 with a grain size of 1 nm was not influenced by the introduction of WA on the surface. TC adsorption was studied as a function of pH, contact time, concentration at incubation, temperature, coexisting ions, and humic acid. The adsorption capacity of the composite was great (273.84 mg g^{-1} at 298 K), and the Langmuir isotherm and pseudo-second order kinetic models reflected the adsorption well. A thermodynamic study of the adsorption determined that it was an endothermic and spontaneous procedure. Moreover, a feasible adsorption mechanism was suggested. The elimination efficiency of TC decreased after 3 cycles, from 94.09% to 80.27%, indicating that the composite can be reused. The measured cobalt leaching was in the acceptable range, indicating that the composite does not cause serious secondary contamination. TC can be effectively removed from water with ZIF-67@WA due to its excellent performance of adsorption, compressibility, light weight, and easy separation (Figure 7) [174].

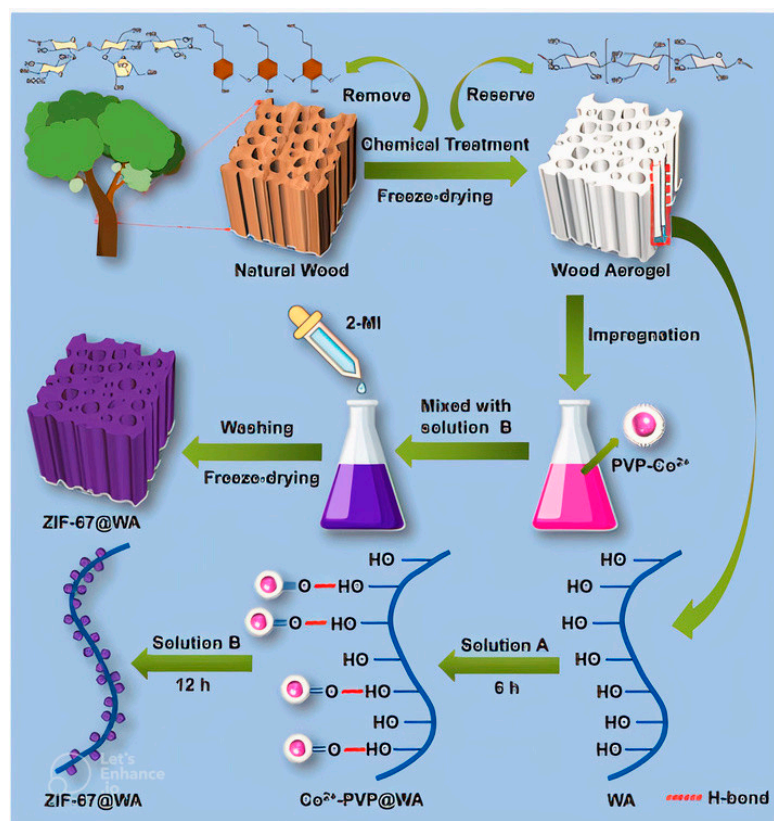


Figure 7. Process of ZIF-67@WA fabrication, reproduced with permission from [174]. Copyright Elsevier, 2021.

6.2. Equilibrium Isotherm and Kinetics Modeling

A significant aspect in the adsorption systems development is the isotherm of adsorption. An adsorption study provides information on how contaminants interact with adsorbents [175]. Consequently, it can have a crucial role in finding the adsorption capacity

and enhancing the adsorbent effectiveness when used in a suitable adsorption system [176]. Different adsorbate concentrations have been used to determine the adsorption isotherms for some synthetic materials [177,178]. In adsorption systems designing, the equilibrium relationships provide information about the surface properties and capacities of adsorbents [179]. The Langmuir, Freundlich, Temkin, and Dubinin–Radushkevich (D-R) isotherm models have been utilized to study adsorption equilibrium data. These models provide important data about the adsorption mechanism [180]. The adsorption equilibrium occurs in the form of a reversible chemical equilibrium among the surface of the adsorbent and the adsorbate solution according to the Langmuir adsorption isotherm model [175]. In this model, adsorption occurs at specific homogeneous sites on the surface of the adsorbent without in-plane diffusion of the adsorbate. The Freundlich isotherm is based on single-layer, reversible, and non-ideal adsorption, which is utilized in multilayer adsorption on heterogeneous surfaces via various adsorption affinities and energies [180]. According to the Temkin isotherm model, the heat of adsorption reduces linearly via increasing the surface coverage of the adsorbent. One of the features of this model is the uniform dispersion of the binding energy. As another empirical model, the Dubinin–Radushkevich isotherm describes the adsorption of molecules on heterogeneous surfaces with a Gaussian energy dispersion [181]. Table 3 shows the Langmuir model explains the experiments more accurately (with $R^2 = 0.999$) [178,180,182,183]. This is because the model has a better correlation coefficient (R^2). However, other statistical ratios besides R^2 should be considered in this evaluation. The model supposes that adsorption happens in a monolayer and is based on the assumption that the surfaces of the adsorbents have active sites with uniform adsorption energies [182,184]. One method of representing the interaction between adsorbents and processes is adsorption kinetics. Optimal operating conditions for a batch adsorption system are determined via kinetic studies [180]. Various pollutions' adsorption kinetics on ZIF have been investigated in a series of experiments. Using the adsorption kinetics to determine the rate of adsorption is important in batch adsorption process designing [185]. To obtain helpful information on the factors influencing the rate of reaction, models of chemical kinetics must totally account for the adsorbent's chemical and physical features [186]. Pseudo-first order and pseudo-second order intraparticle diffusion models were used to find the contaminant adsorption kinetics on ZIFs. In most cases, the pseudo-second order model fits the experimental data best, with R^2 values ranging from 0.9855 to 1.000. A mesopore in ZIF-8/67 increases the adsorption affinity by allowing diffusion of different adsorbates. A second-order kinetic model governing the adsorption rate and adsorption capability based on chemisorption was well fitted to all kinetic curves studied in the work under review [187]. It is obvious that large specific surface areas, porous structures, and active adsorption sites correlate with high adsorption capacity [188]. Owing to the empirical nature of the pseudo-second order model, current derivations of chemisorption have been criticized [189]. According to research carried out by Igwegbe et al., the pseudo-second order model provides insufficient information to indicate the surface heterogeneity of the adsorbent, especially when the linear plot varies [190]. To understand the surface heterogeneity of the adsorbent, a two-sided pseudo-second order model can be utilized. According to this two-sided pseudo-second order model, there are two adsorption sites on the adsorbent, a and b. Adsorption at site a reaches equilibrium earlier than at site b, and adsorption kinetics data at site b follow the pseudo-second order model [191]. The solution initial concentration offers essential details about the driving force that overcomes the adsorbate total resistance during mass transfer among the ZIP surface and the aqueous solution [192]. Thus, a high initial concentration of contaminant accelerates the adsorption procedure. As the pollutant concentration increases, the pollutant molecules diffuse more slowly within the boundary layer and diffuse into the solid's pores [193].

Table 3. Modeling of equilibrium isotherms and kinetics.

ZIFs	Pollutant	Best Kinetics Model	R ²	Best Isotherm Model	R ²	Ref.
ZIF-8/APTMS	Acid blue 92	Pseudo-second order	0.9970	Langmuir	0.9990	[180]
ZIF-8	Trichloroethylene	Pseudo-second order	0.9820	Langmuir	0.9930	[194]
ZIF-67	CR	Pseudo-second order	>0.9000	Freundlich	>0.9700	[193]
CTAB-ZIF-67	Diclofenac	Pseudo-second order	0.9920	Langmuir	0.9930	[195]
ZIF-8/PAN	MB	Pseudo-second order	0.9980	Langmuir	0.9940	[196]
ZIF-67	CIP	Pseudo-second order	0.9990	Langmuir	0.9920	[197]
ZIF-8/PDA/PAN	TC	Pseudo-second order	0.9990	Freundlich	0.9860	[69]

6.3. Photocatalytic Removal of Dyes and Antibiotics by ZIF-8 and ZIF-67

There has been extensive research on using ZIF-8 and ZIF-67 for water contaminant removal using a photocatalytic approach. Using Ag/AgCl NPs anchored on the ZIF-8 surface, Fan and his co-workers provided a composite Ag/AgCl/ZIF-8 in 2017 [198]. Typical procedures include dispersing ZIF-8 evenly in the solution of ZnCl₂, adding AgNO₃ solution, and stirring the prepared suspension for 30 min. In a photo-reduction process, UV-vis light irradiation of white products resulted in an Ag/AgCl/ZIF-8 composite. Ag/AgCl removed approximately 60% of RhB in one hour, whereas Ag/AgCl/ZIF-8 entirely removed the dye. Acetaminophen and MB degradation by the Ag/AgCl/ZIF-8 composite was reported by other researchers [199,200]. Due to their wide energy band, AgCl and ZIF-8 cannot be inspired by visible light illumination in this photocatalytic system, but Ag/AgCl can because of surface plasma resonance. The absorbed photons can then be converted into e⁻ and h⁺ by Ag/AgCl/ZIF-8. Due to Ag NPs' lower Fermi level compared to AgCl, the photoexcited e⁻ will rapidly transfer to Ag NP. The strong adsorption ability of Ag NPs, combined with the power reduction of ZIF-8, would then result in the transfer of the e⁻ on Ag NPs to the CB of ZIF-8, leading to active O₂ generation (Figure 8a) [201,202]. In addition, h⁺ oxidizes Cl⁻ ions in AgCl to produce Cl• radicals, which may also degrade pollutants. With overdose Ag⁺, Fan's research group [203] developed Ag/AgCl/Ag nanofilm/ZIF-8 (AFZ) material. The MB photocatalytic degradation by AFZ was higher than that by Ag/AgCl/ZIF-8 (AZ). Photocatalytic systems AZ and AFZ removed 42.25% and 53.39% of TOC, separately, after 12 min of visible light irradiation. There is evidence that the nanofilm of Ag on ZIF-8 acts like an electronic mediator between ZIF-8 and SPR metallic Ag, allowing e⁻ to be transported from Ag/AgCl to ZIF-8 (Figure 8b) [203]. Separating photoexcited e⁻ more effectively produces an enhanced amount of O₂^{•-}.

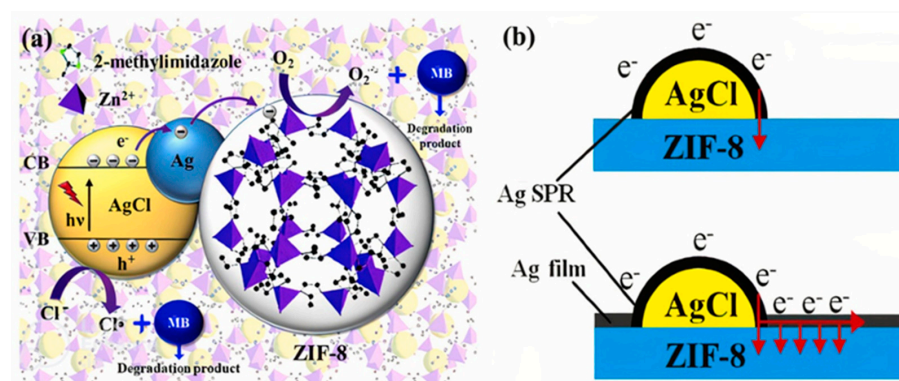


Figure 8. (a) Ag/AgCl/ZIF-8 composite degradation mechanism, reproduced with permission from [200]. Copyright Elsevier, 2018; (b) transfer of electrons from plasmonic metal to AZ and AFZ, reproduced with permission from [203]. Copyright Elsevier, 2017.

Jing et al. investigated the ability of ZIF-8 to eliminate MB under UV light irradiation. The stability and ZIF-8 degradation were also analyzed in terms of the influencing factors, kinetics, and mechanisms. As confirmed by the detection of hydroxyl radicals ($\bullet\text{OH}$) via fluorescence, the ZIF-8 photocatalyst showed efficient photocatalytic activity for the MB degradation under UV irradiation. A pseudo-kinetic first-order model explained the removal of MB by the ZIF-8 photocatalyst. A strong alkaline environment increased the adsorption potential of ZIF-8 and degradation efficiency in a pH range from 4.0 to 12.0. In strong alkaline environments, ZIF-8 works more efficiently due to its higher charge ($\text{pH} > \text{pH}_{\text{pzc}}$) and its higher yield of OH. ZIF-8 could remove MB via photocatalysis. ZIF-8 was considered to be an effective photocatalyst for the organic contaminants decomposing in this study [203]. A TiO_2 @ZIF-8 composite was prepared by encapsulating TiO_2 nanotubes in ZIF-8 and used for visible light dye degradation. ZIF-8 acted as a host during the synthesis to make sure that TiO_2 did not condense. The UV-DRS spectra clearly showed that the microenvironment of TiO_2 nanotubes was modified in the ZIF-8 cages, which decreased the TiO_2 band gap and increased the photocatalytic activity [204]. The paint can be completely removed after 2 h of catalysis. In the case of MB, TiO_2 @ZIF-8 can remove 87.5% of the dye, which is three times faster than TiO_2 nanotubes alone. According to this study, TiO_2 @ZIF-8 had a high rate of recycling in comparison to ZIF-8 and TiO_2 , while TiO_2 nanotubes showed low catalytic efficiency after the second degradation. Using ZnO @ZIF-8 hetero structures, Wang et al. tested the selective photocatalysis function of dye effluent consisting of MB and Cr(VI) [205]. Since ZnO @ZIF-8 exhibited a band gap of 3.3 eV, it was promising that enhanced selective photocatalysis could be achieved. Colloidal ZnO beads were utilized to purify dye sewage, and both Cr(VI) and MB were removed simultaneously, but MB was degraded faster than Cr(VI). MB was entirely eliminated after 80 min, but 50% of Cr(VI) was still present. For the ZnO @ZIF-8 core-shell hetero structures used to purify dye wastewater, photocatalytic selectivity elimination was enhanced over Cr(VI), such that only 12% Cr(VI) was still present after 240 min. In contrast, more than half was left at MB when the equilibrium of degradation was reached after 80 min. The results indicate that ZnO @ZIF-8 was able to selectively photocatalyze Cr(VI) while slowing down the MB decomposing [206]. In another work [207], an ultrasonic cavitation technique was used to prepare ZIF-8-supported BiFeO_3 photocatalysts. SEM and Raman spectroscopy were utilized to characterize the synthesized substances. In this study, the synthesized photocatalysts were evaluated for their ability to decolorize the dye rhodamine-B under ultraviolet and visible light. To understand the role of the photocatalyst in decolorizing rhodamine-B, various operating parameters such as the amount of ZIF-8 in the composite, catalyst dosage, initial concentration of dye, and solution pH were studied at the beginning. The result was that the composite of ZIF-8 and BiFeO_3 at 40.7 wt% showed the best photocatalytic behavior in decolorizing the rhodamine B dye. An acidic pH was more effective in removing Rh-B dye. Compared with ZIF-8 MOF and BiFeO_3 , the hybrid ZIF-8/ BiFeO_3 is more effective in decolorizing Rh-B dye. Under ultraviolet and visible light, the synthesized ZIF-8/ BiFeO_3 demonstrated exceptional photocatalytic activity for Rh-B dye removal from aqueous solutions. Rui Li et al. developed a ZIF-8@ TiO_2 composite using a hydrothermal process. Charge transfer paths were possible between ZIF-8 and TiO_2 due to Zn-O-Ti formation at the interface (Figure 9). By transferring TiO_2 's photogenerated carriers to ZIF-8, O_2 adsorbed on ZIF-8 can be provided with photogenerated electrons, so that more $\bullet\text{O}_2$ was generated. According to an alternative catalytic pathway, TiO_2 photogenerated carriers can react with O_2 and H_2O and produce $\bullet\text{OH}$ and $\bullet\text{O}_2^-$ that could be used to degrade antibiotics. Furthermore, C and N elements were doped into TiO_2 while the composite was being prepared, which reduced the band gap; it would also improve the usage rate of visible light. However, in the mixed materials, ZIF-8 primarily served as an antimicrobial adsorbent, while TiO_2 served as a catalytic agent, and they acted synergistically to remove antibiotics [208].

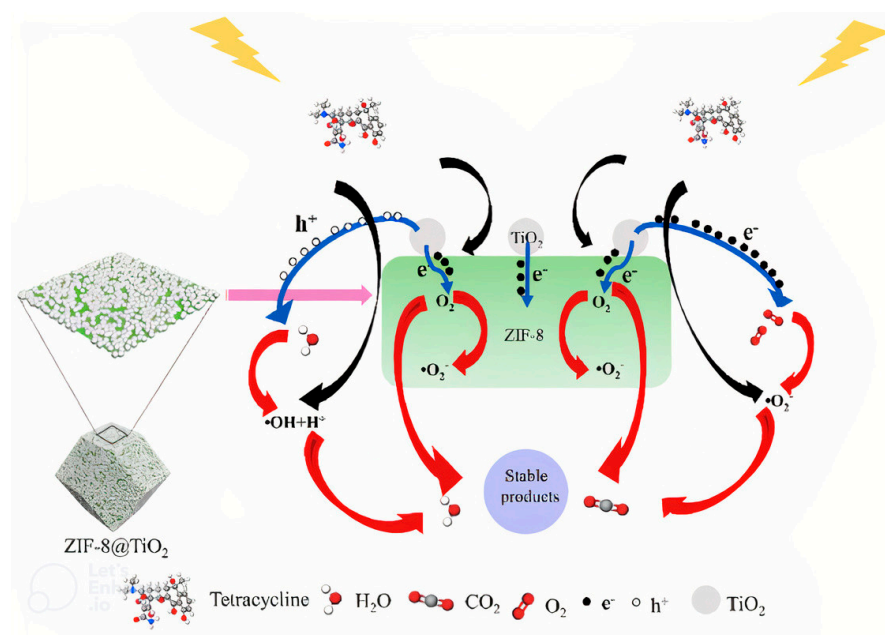


Figure 9. Mechanism of photocatalysis, reproduced with permission from [208]. Copyright Elsevier, 2020.

Dyed organic compounds can be easily removed from water with $\text{Fe}_3\text{O}_4/\text{ZIF-67}$. There are several reasons for this, including a large surface area, the possibility of recycling, and flower-like morphology. In Guan's study, a highly stable $\text{Fe}_3\text{O}_4/\text{ZIF-67}$ nanocomposite was developed using the magnetic properties of Fe_3O_4 and its photocatalytic efficacy for the elimination of Congo red (CR) in the visible light wavelength range. Since Fe_3O_4 NPs were immobilized on ZIF-67, their magnetic effects were rapidly transferred to the external magnetic field, which facilitated their separation from aqueous solutions [209]. In another study, ZIF-67@ CoWO_4 @CoS hetero structures showed good performance in the degradation of dyes under visible light MB. Various surface characterization techniques have been utilized for analyzing the optical, structural, and morphological features of this material, including XRD, FE-SEM, EDX, UV-DRS, VSM, and BET. After 10 min of irradiation, the photocatalyst ZIF-67@ CoWO_4 @CoS showed higher photocatalytic degradation efficiency than its complementary components (about 100%). Moreover, the ZIF-67@ CoWO_4 @CoS photocatalyst showed higher activity than the ZIF-67@ CoWO_4 and ZIF-67@CoS nanocomposites. The produced ZIF-67@ CoWO_4 @CoS hetero structures exhibited enhanced photocatalytic degradation efficiency due to the synergistic impacts of ZIF-67, CoWO_4 , and CoS NPs and the narrow energy band gap. MB is degraded via photocatalysis according to a pseudo-first order kinetic model ($K_1 = 0.1050 \text{ min}^{-1}$). Furthermore, the ZIF-67@ CoWO_4 @CoS photocatalyst showed exceptional stability and could be reused eight times with no significant reduction in its decomposing activity. The study demonstrates the effectiveness, low cost, and easy availability of the ZIF-67@ CoWO_4 @CoS photocatalyst in degrading a variety of organic contaminants in wastewater [210]. Chen et al. developed a composite photocatalyst of molybdenum disulfide and zeolitic imidazolate framework-8 ($\text{MoS}_2/\text{ZIF-8}$), which increased the CIP and TC degradation rates by 1.21 and 1.07, respectively. The catalysis processes tentatively identified the conversion products for CIP and TC. Compared to MoS_2 , the ZIF-8 nanocomposites produce 1.790 times more hydrogen than MoS_2 . In this study, original and effective 1T/2H- MoS_2 /MOF-based photocatalysts were investigated by optimizing the design of the surface nano-heterojunction structures. Stability testing revealed that the assembled photocatalyst is durable and exhibits a high level of catalytic performance. Therefore, the application of photocatalysts based on 1T/2H- MoS_2 /MOF for the degradation of antibiotics is very promising [211]. According to Guo et al., an in-situ co-precipitation process was used to form a direct Z-scheme heterojunction with a coexisting Ag^+/Ag^0 system. By exchanging Ag^+ and Zn^{2+} ions, it was confirmed that Ag^+ and Ag^0 exist on the ZIF-8 surface. The band gap of ZIF-8 decreased in accordance

with X-ray diffraction (XRD) and X-ray photoelectron spectroscopy. In the degradation of antibiotics with multiple residues under visible light irradiation for 60 min, the 12 wt% Ag@ZIF-8/g-C₃N₄ nanocomposites showed the best adsorptive photocatalytic activity. Compared with pure g-C₃N₄, they showed a degradation efficacy of 90% and an apparent 10.27 times higher reaction rate constant. It was demonstrated that $\cdot\text{O}_2^-$ and $\cdot\text{OH}$ have a crucial role in the process of photocatalytic degradation in radical scavenging experiments. Moreover, they proposed that an internal electric field is created to compensate the interfacial mediators among Ag@ZIF-8 and g-C₃N₄, a possible direct photocatalytic Z-scheme mechanism. To achieve this improvement, Ag@ZIF-8 and g-C₃N₄ were prepared in a direct Z-scheme heterojunction. In this way, the redox capability of Ag@ZIF-8/g-C₃N₄ and the electrons and holes separation can be accelerated. The combination of adsorption and photocatalysis is a promising approach for the degradation of various antibiotics. The high surface area and high orienting adsorption capacity of ZIF-8 make it ideal for integrated adsorption-photocatalytic antibiotic removal. Consequently, this investigation provided novel perceptions about improving the redox potential to efficiently degrade several antibiotics under visible light [212]. On the basis of a plain hydrothermal synthesis method based on ZIF-67, Askari et al. constructed a ternary MOF-based heterojunction catalyst from CuWO₄/Bi₂S₃/ZIF-67, and the central conformal design was utilized to find the optimal operating factors of the photocatalytic degradation operation for cephalexin and metronidazole. Under optimal conditions and visible light irradiation, the cephalexin and metronidazole PPCPs showed degradation efficiencies of 90.1% and 95.6%, respectively, with maximum total organic carbon elimination of 74% and 83.20% each. The new triple photocatalytic removal with MOFs has a considerably enhanced performance compared to the binary catalyst CuWO₄/Bi₂S₃ alone [213]. Hou et al. synthesized the ZIF-67 catalyst using Co(NO₃)₂ and 2 MIM at room temperature. Hydrogen peroxide promotes excellent degradation of TC by ZIF-67 catalysts. It was also shown that the concentration of hydrogen peroxide, the catalyst dose, and the dose of TC affected the degradation of TC. The experimental results showed that $\cdot\text{OH}$ was the dominant active species. ZIF-67 was effectively reutilized four times without any significant reduction in degradation efficacy, demonstrating its excellent reusability and stability [214].

7. Desorption and Reusability

Analysis of the reusability and regenerability of a used adsorbent is critical to the possibility of using an adsorbent for industrial applications where cost is an important consideration [215,216]. The commercial usage of the adsorbent technology depends on its reusability degree. This is because the effectiveness of a selected adsorption process increases when the adsorbent is validated for reusability. The recovery of the adsorbent after the uptake of impurities and the continuous utilization of the adsorbent while maintaining its properties after repeated regeneration are also significant features of an adsorbent used in industry [194]. Table 4 summarizes the results of the different adsorbents for ZIFs in terms of desorption and reusability. For example, Panda et al. investigated ZIF-8 to remove reactive blue-4 (RB4) from aqueous media through physical adsorption. In this study, electrostatic attraction, pore-filling effects, and hydrogen bonding interactions were discussed in light of the adsorption of RB4. The adsorption capacity of ZIF-8 for three consecutive adsorption-desorption cycles was compared, and according to the result, ZIF-8's adsorption-desorption capacity decreased by 30% after three cycles [217]. NaCl solutions have also been used to revive ZIFs for electrostatic adsorption of contaminants through the electrostatic attraction force. During washing of used ZIF-67, Seo et al. used a high concentration of NaCl (15 wt%) as the eluent. The results showed that rinsing with NaCl solution can demonstrate good and stable regeneration efficiency upon multiple cycles of analysis [218]. Several researchers have also used C₂H₅OH as an eluent for washing used ZIFs. Lin et al. used MRGO/ZIF for the removal of MG. Multiple-cycle MG adsorption using regenerated MRGO/ZIF revealed that MRGO/ZIF can be recovered and reused, demonstrating high efficiency and stability of the recyclability. The rate of its adsorption after four cycles was 100% [219]. Due to

their excellent regeneration properties, ZIF-8/ZIF-67 were excellent adsorbents for the elimination of various pollutants from polluted water. Various methods were used to study the desorption of contaminants from spent ZIFs such as the use of different eluents and pH variations in aqueous solutions [138]. By washing the adsorbents utilized with eluents such as NaOH [180,220], methanol [221], acidic ethanol [222], NaCl [223], ethanol [217,223], and HCl [223], etc., ZIFs can be regenerated. ZIFs can be regenerated and reused for further adsorption processes; they are then filtered and dried for recovery.

Table 4. Rate of desorption, adsorption of ZIF-8 and ZIF-67.

Type of ZIFs	Pollution	Eluent	Rate of Desorption	Cycle Number	Rate of Adsorption after N Cycles	Ref.
ZIF-8	Reactive blue-4	C ₂ H ₅ OH	-	3	70	[217]
ZIF-67	CR	C ₂ H ₅ OH	-	3	90	[223]
ZIF-8/APTMS	Acid blue 92	NaOH	100	4	82	[180]
ZIF-8/PAN	MB	C ₂ H ₅ OH	-	3	85	[196]
ZIF-8	CIP	CH ₃ OH	97	7	85	[188]
ZIF-67	CIP	C ₂ H ₅ OH	-	5	80	[197]
CTAB-ZIF-67	Diclofenac	NaCl	-	-	80	[218]
MRGO-ZIF-67	MG	C ₂ H ₅ OH	98	4	100	[222]

8. Perspective

Despite the extensive and ongoing research on dye and antibiotic adsorption and photocatalytic degradation by ZIFs, further attention should be paid to practical applications. With respect to dyes and antibiotics, ZIFs face several critical challenges in practice:

1. Any research result must not only be socially and environmentally friendly, but also be transferred from laboratory research to industrial application. Therefore, in addition to capacity of adsorption and degradation, selectivity adsorption, photodegradation of pollutants, and recyclability are critical for practical application. To optimize the ZIF-8/67 composites for photocatalytic elimination of pollutions, future studies should improve the adsorption efficacy of sunlight and minimize electron-hole pair recombination. Production cost remains a bottleneck in the industrialization of ZIF-8/67 as a key evaluation metric in engineering applications. On the other hand, a ZIF-8/67 composite must withstand acidic situations, high temperatures, and complex organic solvent systems and must exhibit long-term water stability in wastewater treatment. Therefore, more cost-effective synthesis strategies need to be developed and composites recycled.
2. MOFs (ZIFs) are currently used to remove antibiotics and dyes from laboratory beakers. In the future, it is expected that these materials will be utilized in reactors and even water purification plants. The problem appears to be solved by combining ZIF-based photocatalysts with membrane reactors and support-based adsorbents. It is not only water quality that is threatened by antibiotics. As a result of the accumulation of antibiotics in water, microbial resistance genes are formed. Currently, resistance genes limited to ZIF-8/67 have not been researched in depth.
3. Current research focuses on the removal of antibiotics in the mg/L range. Nevertheless, most antibiotics in natural waterbodies and urban wastewater are dissolved at concentrations of µg/L, making the application of ZIFs for adsorption and photocatalytic antibiotics removal difficult.
4. While the rate of antibiotics and dyes removal is hopeful when processed with ZIF-8/67, the removal rate of COD is relatively low, indicating that antibiotics and dyes are not mineralized to their maximum potential. Many intermediates are

involved in the photodegradation process, so the research of the intermediates is also important.

9. Conclusions

MOFs are very efficient in adsorption and photodegradation due to their composition of metals or metal clusters and organic coupling agents. The efficiency of MOFs can be improved by enhancing their pore structure, functionality, and metal doping. Because of their excellent thermal and chemical stability, ZIF-8 and ZIF-67 are successful materials for wastewater treatment and can overcome the drawbacks of MOFs. ZIF-8/67 composites are gaining popularity in water purification and wastewater remediation owing to their high porosity and active sites. However, there are some weaknesses, especially in terms of the synthesis cost of ZIFs and the problem of secondary pollution of the environment, which may result from ZIFs entering water during wastewater treatment. Using environmentally friendly approaches, such as a hydrothermal process for preparation of ZIFs, can be very cost-effective, and bonding ZIFs with effortlessly reusable magnetic materials, mixing ZIFs with filter membranes, and applying ZIFs to macrosubstrates can solve these significant limitations, respectively.

Here, we reviewed the literature on the application of ZIF-8/67 as adsorbent and photocatalyst for the elimination of water contaminants such as dyes and antibiotics, followed by an introduction to the synthesis strategies for ZIF-8/67 composites and their general application. Accordingly, further studies should aim to determine the mechanism of biological effects of ZIF-8/67, allowing fine-tuning at the molecular level and, consequently, effective action on biological targets and minimal toxicity. In addition, biomedical research should be conducted with solution-stable MOFs under physiological circumstances and concentrations.

Author Contributions: Z.P. and S.M.M. developed the idea and structure of the review article. S.A.H., A.B., Z.P., Y.M. and C.W.L. wrote the manuscript, collecting the materials from databases, and revised and improved the manuscript. S.M.M. and W.-H.C. supervised the manuscript. All authors have read and agreed to the published version of the manuscript.

Funding: This research received no external funding.

Data Availability Statement: Not applicable.

Conflicts of Interest: The authors declare no conflict of interest.

References

1. Shannon, M.A.; Bohn, P.W.; Elimelech, M.; Georgiadis, J.G.; Marinas, B.J.; Mayes, A.M. Science and technology for water purification in the coming decades. *Nanosci. Technol. A Collect. Rev. Nat. J.* **2010**, *7185*, 337–346.
2. Vörösmarty, C.J.; McIntyre, P.B.; Gessner, M.O.; Dudgeon, D.; Prusevich, A.; Green, P.; Glidden, S.; Bunn, S.E.; Sullivan, C.A.; Liermann, C.R. Global threats to human water security and river biodiversity. *Nature* **2010**, *467*, 555–561. [[CrossRef](#)] [[PubMed](#)]
3. Pouramini, Z. The VOCs catalytic combustion by perovskite catalysts: A mini-review. *Adv. Appl. NanoBio-Technol.* **2022**, *3*, 23–30.
4. Lapworth, D.; Baran, N.; Stuart, M.; Ward, R. Emerging organic contaminants in groundwater: A review of sources, fate and occurrence. *Environ. Pollut.* **2012**, *163*, 287–303. [[CrossRef](#)] [[PubMed](#)]
5. Liang, W.; Wang, B.; Cheng, J.; Xiao, D.; Xie, Z.; Zhao, J. 3D, eco-friendly metal-organic frameworks@ carbon nanotube aerogels composite materials for removal of pesticides in water. *J. Hazard. Mater.* **2021**, *401*, 123718. [[CrossRef](#)]
6. Naskar, J.; Boatemaa, M.A.; Rumjit, N.P.; Thomas, G.; George, P.; Lai, C.W.; Mousavi, S.M.; Wong, Y.H. Recent Advances of Nanotechnology in Mitigating Emerging Pollutants in Water and Wastewater: Status, Challenges, and Opportunities. *Water Air Soil Pollut.* **2022**, *233*, 156. [[CrossRef](#)]
7. Joseph, L.; Jun, B.-M.; Jang, M.; Park, C.M.; Muñoz-Senmache, J.C.; Hernández-Maldonado, A.J.; Heyden, A.; Yu, M.; Yoon, Y. Removal of contaminants of emerging concern by metal-organic framework nanoadsorbents: A review. *Chem. Eng. J.* **2019**, *369*, 928–946. [[CrossRef](#)]
8. Sharma, S.; Kaur, A. Various methods for removal of dyes from industrial effluents—A review. *Indian J. Sci. Technol* **2018**, *11*, 1–21. [[CrossRef](#)]
9. Pouramini, Z.; Ayati, B.; Babapoor, A. Enhancing PFC ability to dye removal and power generation simultaneously via conductive spheres in the anodic chamber. *J. Electroanal. Chem.* **2022**, *917*, 116410. [[CrossRef](#)]

10. Brazesh, B.; Mousavi, S.M.; Zarei, M.; Ghaedi, M.; Bahrani, S.; Hashemi, S.A. Biosorption. In *Interface Science and Technology*; Elsevier: Amsterdam, The Netherlands, 2021; Volume 33, pp. 587–628.
11. Hashemi, S.A.; Mousavi, S.M.; Ramakrishna, S. Effective removal of mercury, arsenic and lead from aqueous media using Polyaniline-Fe₃O₄-silver diethyldithiocarbamate nanostructures. *J. Clean. Prod.* **2019**, *239*, 118023. [[CrossRef](#)]
12. Wang, C.; Yin, Y. Preparation, Characterization and Application of Ultra-Fine Modified Pigment in Textile Dyeing. In *Eco-Friendly Textile Dyeing and Finishing*; IntechOpen: London, UK, 2013.
13. Solís, M.; Solís, A.; Pérez, H.I.; Manjarrez, N.; Flores, M. Microbial decolouration of azo dyes: A review. *Process Biochem.* **2012**, *47*, 1723–1748. [[CrossRef](#)]
14. Bouabidi, Z.B.; El-Naas, M.H.; Cortes, D.; McKay, G.J.C.E.J. Steel-Making dust as a potential adsorbent for the removal of lead (II) from an aqueous solution. *Chem. Eng. J.* **2018**, *334*, 837–844. [[CrossRef](#)]
15. Saravanan, S.; Kumar, P.S.; Chitra, B.; Rangasamy, G. Biodegradation of textile dye Rhodamine-B by *Brevundimonas diminuta* and screening of their breakdown metabolites. *Chemosphere* **2022**, *308*, 136266. [[CrossRef](#)] [[PubMed](#)]
16. Hashemi, S.A.; Bahrani, S.; Mousavi, S.M.; Mojoudi, F.; Omidifar, N.; Lankarani, K.B.; Arjmand, M.; Ramakrishna, S. Development of sulfurized Polythiophene-Silver Iodide-Diethyldithiocarbamate nanoflakes toward Record-High and selective absorption and detection of mercury derivatives in aquatic substrates. *Chem. Eng. J.* **2022**, *440*, 135896. [[CrossRef](#)]
17. Gupta, V. Application of low-cost adsorbents for dye removal—a review. *J. Environ. Manag.* **2009**, *90*, 2313–2342.
18. Amini, Z.P.J.A.i.A.N.-T. Using nanomembrane to heavy metal removal from wastewater: A mini-review. *Adv. NanoBio-Technol.* **2022**, *3*, 7–13.
19. Uddin, M.J.; Ampiauw, R.E.; Lee, W. Adsorptive removal of dyes from wastewater using a metal-organic framework: A review. *Chemosphere* **2021**, *284*, 131314. [[CrossRef](#)]
20. Massé, D.I.; Cata Saady, N.M.; Gilbert, Y. Potential of biological processes to eliminate antibiotics in livestock manure: An overview. *Animals* **2014**, *4*, 146–163. [[CrossRef](#)]
21. Klein, E.Y.; Van Boeckel, T.P.; Martinez, E.M.; Pant, S.; Gandra, S.; Levin, S.A.; Goossens, H.; Laxminarayan, R. Global increase and geographic convergence in antibiotic consumption between 2000 and 2015. *Proc. Natl. Acad. Sci. USA* **2018**, *115*, E3463–E3470. [[CrossRef](#)]
22. Reardon, S. Antibiotic resistance sweeping developing world: Bacteria are increasingly dodging extermination as drug availability outpaces regulation. *Nature* **2014**, *509*, 141–143. [[CrossRef](#)]
23. Zeng, G.; Chen, M.; Zeng, Z. Risks of neonicotinoid pesticides. *Science* **2013**, *340*, 1403. [[CrossRef](#)] [[PubMed](#)]
24. Xu, J.; Shen, X.; Jia, L.; Zhou, T.; Ma, T.; Xu, Z.; Cao, J.; Ge, Z.; Bi, N.; Zhu, T. A novel visual ratiometric fluorescent sensing platform for highly-sensitive visual detection of tetracyclines by a lanthanide-functionalized palygorskite nanomaterial. *J. Hazard. Mater.* **2018**, *342*, 158–165. [[CrossRef](#)]
25. Buonomenna, M.G.; Mousavi, S.M.; Hashemi, S.A.; Lai, C.W. Water Cleaning Adsorptive Membranes for Efficient Removal of Heavy Metals and Metalloids. *Water* **2022**, *14*, 2718. [[CrossRef](#)]
26. Sharma, B.M.; Bečanová, J.; Scheringer, M.; Sharma, A.; Bharat, G.K.; Whitehead, P.G.; Klánová, J.; Nizzetto, L. Health and ecological risk assessment of emerging contaminants (pharmaceuticals, personal care products, and artificial sweeteners) in surface and groundwater (drinking water) in the Ganges River Basin, India. *Sci. Total Environ.* **2019**, *646*, 1459–1467. [[CrossRef](#)] [[PubMed](#)]
27. Jurado, A.; Walther, M.; Díaz-Cruz, M.S. Occurrence, fate and environmental risk assessment of the organic microcontaminants included in the Watch Lists set by EU Decisions 2015/495 and 2018/840 in the groundwater of Spain. *Sci. Total Environ.* **2019**, *663*, 285–296. [[CrossRef](#)] [[PubMed](#)]
28. TaheriAshtiani, N.; Ayati, B. Using chitosan-based heterogeneous catalyst for degradation of Acid Blue 25 in the effective electro-Fenton process with rotating cathodes. *J. Electroanal. Chem.* **2022**, *905*, 115983. [[CrossRef](#)]
29. Vickers, N.J. Animal communication: When i’m calling you, will you answer too? *Curr. Biol.* **2017**, *27*, R713–R715. [[CrossRef](#)] [[PubMed](#)]
30. Yang, Z.-H.; Cao, J.; Chen, Y.-P.; Li, X.; Xiong, W.-P.; Zhou, Y.-Y.; Zhou, C.-Y.; Xu, R.; Zhang, Y.-R. Mn-doped zirconium metal-organic framework as an effective adsorbent for removal of tetracycline and Cr (VI) from aqueous solution. *Microporous Mesoporous Mater.* **2019**, *277*, 277–285. [[CrossRef](#)]
31. Cheng, Y.; He, H.; Yang, C.; Zeng, G.; Li, X.; Chen, H.; Yu, G. Challenges and solutions for biofiltration of hydrophobic volatile organic compounds. *Biotechnol. Adv.* **2016**, *34*, 1091–1102. [[CrossRef](#)]
32. Aoudj, S.; Khelifa, A.; Drouiche, N.; Belkada, R.; Miroud, D.J.C.E.J. Simultaneous removal of chromium (VI) and fluoride by electrocoagulation–electroflotation: Application of a hybrid Fe-Al anode. *Chem. Eng. J.* **2015**, *267*, 153–162. [[CrossRef](#)]
33. Cheng, M.; Zeng, G.; Huang, D.; Lai, C.; Xu, P.; Zhang, C.; Liu, Y. Hydroxyl radicals based advanced oxidation processes (AOPs) for remediation of soils contaminated with organic compounds: A review. *Chem. Eng. J.* **2016**, *284*, 582–598. [[CrossRef](#)]
34. Masood, Z.; Ikhtlaq, A.; Akram, A.; Qazi, U.Y.; Rizvi, O.S.; Javaid, R.; Alazmi, A.; Madkour, M.; Qi, F. Application of nanocatalysts in advanced oxidation processes for wastewater purification: Challenges and future prospects. *Catalysts* **2022**, *12*, 741. [[CrossRef](#)]
35. Aghajani, M.; Torabi, S.A.; Heydari, J.J.S.-E.P.S. A novel option contract integrated with supplier selection and inventory prepositioning for humanitarian relief supply chains. *Socio-Econ. Plan. Sci.* **2020**, *71*, 100780. [[CrossRef](#)]

36. Stylianou, M.; Christou, A.; Michael, C.; Agapiou, A.; Papanastasiou, P.; Fatta-Kassinos, D. Adsorption and removal of seven antibiotic compounds present in water with the use of biochar derived from the pyrolysis of organic waste feedstocks. *J. Environ. Chem. Eng.* **2021**, *9*, 105868. [[CrossRef](#)]
37. Qin, K.; Zhao, Q.; Yu, H.; Xia, X.; Li, J.; He, S.; Wei, L.; An, T. A review of bismuth-based photocatalysts for antibiotic degradation: Insight into the photocatalytic degradation performance, pathways and relevant mechanisms. *Environ. Res.* **2021**, *199*, 111360. [[CrossRef](#)]
38. Montes-Hernandez, G.; Concha-Lozano, N.; Renard, F.; Quirico, E. Removal of oxyanions from synthetic wastewater via carbonation process of calcium hydroxide: Applied and fundamental aspects. *J. Hazard. Mater.* **2009**, *166*, 788–795. [[CrossRef](#)]
39. Wang, J.; Dong, S.; Yu, C.; Han, X.; Guo, J.; Sun, J. An efficient MoO₃ catalyst for in-practical degradation of dye wastewater under room conditions. *Catal. Commun.* **2017**, *92*, 100–104. [[CrossRef](#)]
40. Chong, M.N.; Jin, B.; Chow, C.W.; Saint, C. Recent developments in photocatalytic water treatment technology: A review. *Water Res.* **2010**, *44*, 2997–3027. [[CrossRef](#)]
41. Zhang, J.; Si, M.; Jiang, L.; Yuan, X.; Yu, H.; Wu, Z.; Li, Y.; Guo, J. Core-shell Ag@ nitrogen-doped carbon quantum dots modified BiVO₄ nanosheets with enhanced photocatalytic performance under Vis-NIR light: Synergism of molecular oxygen activation and surface plasmon resonance. *Chem. Eng. J.* **2021**, *410*, 128336. [[CrossRef](#)]
42. Mousavi, S.M.; Hashemi, S.A.; Esmaili, H.; Amani, A.M.; Mojoudi, F. Synthesis of Fe₃O₄ nanoparticles modified by oak shell for treatment of wastewater containing Ni (II). *Acta Chim. Slov.* **2018**, *65*, 750–756. [[CrossRef](#)]
43. Azhdari, R.; Mousavi, S.M.; Hashemi, S.A.; Bahrani, S.; Ramakrishna, S. Decorated graphene with aluminum fumarate metal organic framework as a superior non-toxic agent for efficient removal of Congo Red dye from wastewater. *J. Environ. Chem. Eng.* **2019**, *7*, 103437. [[CrossRef](#)]
44. Dai, H.; Yuan, X.; Jiang, L.; Wang, H.; Zhang, J.; Zhang, J.; Xiong, T. Recent advances on ZIF-8 composites for adsorption and photocatalytic wastewater pollutant removal: Fabrication, applications and perspective. *Coord. Chem. Rev.* **2021**, *441*, 213985. [[CrossRef](#)]
45. Dong, W.; Wang, D.; Wang, H.; Li, M.; Chen, F.; Jia, F.; Yang, Q.; Li, X.; Yuan, X.; Gong, J. Facile synthesis of In₂S₃/UiO-66 composite with enhanced adsorption performance and photocatalytic activity for the removal of tetracycline under visible light irradiation. *J. Colloid Interface Sci.* **2019**, *535*, 444–457. [[CrossRef](#)] [[PubMed](#)]
46. Liu, B.; Pouramini, S. Multi-objective optimization for thermal comfort enhancement and greenhouse gas emission reduction in residential buildings applying retrofitting measures by an Enhanced Water Strider Optimization Algorithm: A case study. *Energy Rep.* **2021**, *7*, 1915–1929. [[CrossRef](#)]
47. Qin, L.; Li, Y.; Liang, F.; Li, L.; Lan, Y.; Li, Z.; Lu, X.; Yang, M.; Ma, D. A microporous 2D cobalt-based MOF with pyridyl sites and open metal sites for selective adsorption of CO₂. *Microporous Mesoporous Mater.* **2022**, *341*, 112098. [[CrossRef](#)]
48. Li, L.; Zou, J.; Han, Y.; Liao, Z.; Lu, P.; Nezamzadeh-Ejhi, A.; Liu, J.; Peng, Y. Recent advances in Al (iii)/In (iii)-based MOFs for the detection of pollutants. *New J. Chem.* **2022**, *46*, 19577–19592. [[CrossRef](#)]
49. Liu, J.-Q.; Chen, J.; Cheng, F.; Luo, D.; Huang, J.; Ouyang, J.; Nezamzadeh-Ejhi, A.; Peng, Y.; Khan, M.S. Recent advances in Ti-based MOFs in the biomedical applications. *Dalton Trans.* **2022**, *51*, 14817–14832.
50. Zhang, W.; Ye, G.; Liao, D.; Chen, X.; Lu, C.; Nezamzadeh-Ejhi, A.; Khan, M.S.; Liu, J.; Pan, Y.; Dai, Z. Recent Advances of Silver-Based Coordination Polymers on Antibacterial Applications. *Molecules* **2022**, *27*, 7166. [[CrossRef](#)]
51. Qin, L.; Liang, F.; Li, Y.; Wu, J.; Guan, S.; Wu, M.; Xie, S.; Luo, M.; Ma, D. A 2D Porous Zinc-Organic Framework Platform for Loading of 5-Fluorouracil. *Inorganics* **2022**, *10*, 202. [[CrossRef](#)]
52. Park, K.S.; Ni, Z.; Côté, A.P.; Choi, J.Y.; Huang, R.; Uribe-Romo, F.J.; Chae, H.K.; O’Keeffe, M.; Yaghi, O.M. Exceptional chemical and thermal stability of zeolitic imidazolate frameworks. *Proc. Natl. Acad. Sci. USA* **2006**, *103*, 10186–10191. [[CrossRef](#)]
53. Cheng, N.; Ren, L.; Xu, X.; Du, Y.; Dou, S.X. Recent development of zeolitic imidazolate frameworks (ZIFs) derived porous carbon based materials as electrocatalysts. *Adv. Energy Mater.* **2018**, *8*, 1801257. [[CrossRef](#)]
54. Zhong, G.; Liu, D.; Zhang, J. The application of ZIF-67 and its derivatives: Adsorption, separation, electrochemistry and catalysts. *J. Mater. Chem. A* **2018**, *6*, 1887–1899. [[CrossRef](#)]
55. Mousavi, S.M.; Hashemi, S.A.; Bahrani, S.; Mosleh, S.; Chiang, W.-H.; Yousefi, K.; Ramakrishna, S.; Wei, L.C.; Omidifar, N. Hybrid of sodium polytungstate polyoxometalate supported by the green substrate for photocatalytic degradation of auramine-O dye. *Environ. Sci. Pollut. Res.* **2022**, *29*, 56055–56067. [[CrossRef](#)] [[PubMed](#)]
56. Darvish, M.; Pouramini, M.; Bahador, H. Towards Fine-grained Image Classification with Generative Adversarial Networks and Facial Landmark Detection. Proceedings of 2022 International Conference on Machine Vision and Image Processing (MVIP), Hong Kong, China, 25–27 March 2022; pp. 1–6.
57. Zhong, Y.; Chen, C.; Liu, S.; Lu, C.; Liu, D.; Pan, Y.; Sakiyama, H.; Muddassir, M.; Liu, J. A new magnetic adsorbent of eggshell-zeolitic imidazolate framework for highly efficient removal of norfloxacin. *Dalton Trans.* **2021**, *50*, 18016–18026. [[CrossRef](#)] [[PubMed](#)]
58. Liu, Y.; Cheng, H.; Cheng, M.; Liu, Z.; Huang, D.; Zhang, G.; Shao, B.; Liang, Q.; Luo, S.; Wu, T. The application of Zeolitic imidazolate frameworks (ZIFs) and their derivatives based materials for photocatalytic hydrogen evolution and pollutants treatment. *Chem. Eng. J.* **2021**, *417*, 127914. [[CrossRef](#)]
59. Phan, A.; Doonan, C.J.; Uribe-Romo, F.J.; Knobler, C.B.; O’keeffe, M.; Yaghi, O.M. Synthesis, structure, and carbon dioxide capture properties of zeolitic imidazolate frameworks. *Acc. Chem. Res.* **2010**, *43*, 58–67. [[CrossRef](#)]

60. Wu, R.; Fan, T.; Chen, J.; Li, Y. Synthetic factors affecting the scalable production of zeolitic imidazolate frameworks. *ACS Sustain. Chem. Eng.* **2019**, *7*, 3632–3646. [[CrossRef](#)]
61. Rowsell, J.L.; Yaghi, O.M. Metal–organic frameworks: A new class of porous materials. *Microporous Mesoporous Mater.* **2004**, *73*, 3–14. [[CrossRef](#)]
62. Hu, P.; Morabito, J.V.; Tsung, C.-K. Core–shell catalysts of metal nanoparticle core and metal–organic framework shell. *ACS Catal.* **2014**, *4*, 4409–4419. [[CrossRef](#)]
63. Liu, J.; Thallapally, P.K.; McGrail, B.P.; Brown, D.R.; Liu, J. Progress in adsorption-based CO₂ capture by metal–organic frameworks. *Chem. Soc. Rev.* **2012**, *41*, 2308–2322. [[CrossRef](#)]
64. Li, J.-R.; Kuppler, R.J.; Zhou, H.-C. Selective gas adsorption and separation in metal–organic frameworks. *Chem. Soc. Rev.* **2009**, *38*, 1477–1504. [[CrossRef](#)] [[PubMed](#)]
65. Cavka, J.H.; Jakobsen, S.; Olsbye, U.; Guillou, N.; Lamberti, C.; Bordiga, S.; Lillerud, K.P. A new zirconium inorganic building brick forming metal organic frameworks with exceptional stability. *J. Am. Chem. Soc.* **2008**, *130*, 13850–13851. [[CrossRef](#)] [[PubMed](#)]
66. Li, X.; Liu, Y.; Wang, J.; Gascon, J.; Li, J.; Van der Bruggen, B. Metal–organic frameworks based membranes for liquid separation. *Chem. Soc. Rev.* **2017**, *46*, 7124–7144. [[CrossRef](#)]
67. Li, J.; Wang, H.; Yuan, X.; Zhang, J.; Chew, J.W. Metal-organic framework membranes for wastewater treatment and water regeneration. *Coord. Chem. Rev.* **2020**, *404*, 213116. [[CrossRef](#)]
68. Nozari, V.; Calahoo, C.; Tuffnell, J.M.; Adelman, P.; Wondraczek, K.; Dutton, S.E.; Bennett, T.D.; Wondraczek, L. Sodium ion conductivity in superionic il-impregnated metal-organic frameworks: Enhancing stability through structural disorder. *Sci. Rep.* **2020**, *10*, 3532. [[CrossRef](#)]
69. Chao, S.; Li, X.; Li, Y.; Wang, Y.; Wang, C. Preparation of polydopamine-modified zeolitic imidazolate framework-8 functionalized electrospun fibers for efficient removal of tetracycline. *J. Colloid Interface Sci.* **2019**, *552*, 506–516. [[CrossRef](#)] [[PubMed](#)]
70. Gao, Q.; Xu, J.; Bu, X.-H. Recent advances about metal-organic frameworks in the removal of pollutants from wastewater. *Coord. Chem. Rev.* **2019**, *378*, 17–31. [[CrossRef](#)]
71. Furukawa, H.; Cordova, K.E.; O’Keeffe, M.; Yaghi, O.M. The chemistry and applications of metal-organic frameworks. *Science* **2013**, *341*, 1230444. [[CrossRef](#)]
72. Wen, J.; Fang, Y.; Zeng, G. Progress and prospect of adsorptive removal of heavy metal ions from aqueous solution using metal–organic frameworks: A review of studies from the last decade. *Chemosphere* **2018**, *201*, 627–643. [[CrossRef](#)]
73. Milburn, K. Synthesis and Characterization of ZIF-8 and ZIF-8/Polymer Composites. Ph.D. Dissertation, University of Liverpool, Liverpool, UK, 2000.
74. Song, Z.; Cheng, N.; Lushington, A.; Sun, X. Recent progress on MOF-derived nanomaterials as advanced electrocatalysts in fuel cells. *Catalysts* **2016**, *6*, 116. [[CrossRef](#)]
75. Tchinsa, A.; Hossain, M.F.; Wang, T.; Zhou, Y. Removal of organic pollutants from aqueous solution using metal organic frameworks (MOFs)-based adsorbents: A review. *Chemosphere* **2021**, *284*, 131393. [[CrossRef](#)] [[PubMed](#)]
76. Chen, B.; Yang, Z.; Zhu, Y.; Xia, Y. Zeolitic imidazolate framework materials: Recent progress in synthesis and applications. *J. Mater. Chem. A* **2014**, *2*, 16811–16831. [[CrossRef](#)]
77. Yao, J.; Wang, H. Zeolitic imidazolate framework composite membranes and thin films: Synthesis and applications. *Chem. Soc. Rev.* **2014**, *43*, 4470–4493. [[CrossRef](#)] [[PubMed](#)]
78. Hassan, N.; Shahat, A.; El-Didamony, A.; El-Desouky, M.; El-Bindary, A. Synthesis and characterization of ZnO nanoparticles via zeolitic imidazolate framework-8 and its application for removal of dyes. *J. Mol. Struct.* **2020**, *1210*, 128029. [[CrossRef](#)]
79. Zhang, N.; Zhou, T.; Chen, M.; Feng, H.; Yuan, R.; Yan, W.; Tian, Y.; Wu, X.; Chu, W.; Wu, C. High-purity pyrrole-type FeN₄ sites as a superior oxygen reduction electrocatalyst. *Energy Environ. Sci.* **2020**, *13*, 111–118. [[CrossRef](#)]
80. Huang, X.C.; Lin, Y.Y.; Zhang, J.P.; Chen, X.M. Ligand-directed strategy for zeolite-type metal-organic frameworks: Zinc (II) imidazolates with unusual zeolitic topologies. *Angew. Chem. Int. Ed.* **2006**, *45*, 1557–1559. [[CrossRef](#)]
81. Venna, S.R.; Jasinski, J.B.; Carreon, M.A. Structural evolution of zeolitic imidazolate framework-8. *J. Am. Chem. Soc.* **2010**, *132*, 18030–18033. [[CrossRef](#)]
82. Banerjee, R.; Phan, A.; Wang, B.; Knobler, C.; Furukawa, H.; O’Keeffe, M.; Yaghi, O.M. High-throughput synthesis of zeolitic imidazolate frameworks and application to CO₂ capture. *Science* **2008**, *319*, 939–943. [[CrossRef](#)]
83. Banerjee, R.; Furukawa, H.; Britt, D.; Knobler, C.; O’Keeffe, M.; Yaghi, O.M. Control of pore size and functionality in isorecticular zeolitic imidazolate frameworks and their carbon dioxide selective capture properties. *J. Am. Chem. Soc.* **2009**, *131*, 3875–3877. [[CrossRef](#)]
84. Troyano, J.; Carné-Sánchez, A.; Avci, C.; Imaz, I.; Maspoch, D. Colloidal metal–organic framework particles: The pioneering case of ZIF-8. *Chem. Soc. Rev.* **2019**, *48*, 5534–5546. [[CrossRef](#)]
85. Wang, L.; Guan, Y.; Qiu, X.; Zhu, H.; Pan, S.; Yu, M.; Zhang, Q. Efficient ferrite/Co/porous carbon microwave absorbing material based on ferrite@ metal–organic framework. *Chem. Eng. J.* **2017**, *326*, 945–955. [[CrossRef](#)]
86. Kong, W.; Li, J.; Chen, Y.; Ren, Y.; Guo, Y.; Niu, S.; Yang, Y. ZIF-67-derived hollow nanocages with layered double oxides shell as high-efficiency catalysts for CO oxidation. *Appl. Surf. Sci.* **2018**, *437*, 161–168. [[CrossRef](#)]
87. Wang, C.; Yang, F.; Sheng, L.; Yu, J.; Yao, K.; Zhang, L.; Pan, Y. Zinc-substituted ZIF-67 nanocrystals and polycrystalline membranes for propylene/propane separation. *Chem. Commun.* **2016**, *52*, 12578–12581. [[CrossRef](#)] [[PubMed](#)]

88. Yang, Q.; Ren, S.; Zhao, Q.; Lu, R.; Hang, C.; Chen, Z.; Zheng, H. Selective separation of methyl orange from water using magnetic ZIF-67 composites. *Chem. Eng. J.* **2018**, *333*, 49–57. [CrossRef]
89. Zhan, W.-W.; Kuang, Q.; Zhou, J.-Z.; Kong, X.-J.; Xie, Z.-X.; Zheng, L.-S. Semiconductor@ metal–organic framework core–shell heterostructures: A case of ZnO@ ZIF-8 nanorods with selective photoelectrochemical response. *J. Am. Chem. Soc.* **2013**, *135*, 1926–1933. [PubMed]
90. Falcaro, P.; Ricco, R.; Yazdi, A.; Imaz, I.; Furukawa, S.; MasPOCH, D.; Ameloot, R.; Evans, J.D.; Doonan, C.J. Application of metal and metal oxide nanoparticles@ MOFs. *Coord. Chem. Rev.* **2016**, *307*, 237–254. [CrossRef]
91. Lu, G.; Li, S.; Guo, Z.; Farha, O.K.; Hauser, B.G.; Qi, X.; Wang, Y.; Wang, X.; Han, S.; Liu, X. Imparting functionality to a metal–organic framework material by controlled nanoparticle encapsulation. *Nat. Chem.* **2012**, *4*, 310–316. [CrossRef]
92. Li, T.; Zhang, W.; Zhai, S.; Gao, G.; Ding, J.; Zhang, W.; Liu, Y.; Zhao, X.; Pan, B.; Lv, L. Efficient removal of nickel (II) from high salinity wastewater by a novel PAA/ZIF-8/PVDF hybrid ultrafiltration membrane. *Water Res.* **2018**, *143*, 87–98. [CrossRef]
93. Zhu, Q.-L.; Xu, Q. Metal–organic framework composites. *Chem. Soc. Rev.* **2014**, *43*, 5468–5512. [CrossRef]
94. Huang, X.; Zhang, J.; Chen, X. [Zn(bim)₂](H₂O) 1.67: A metal–organic open-framework with sodalite topology. *Chin. Sci. Bull.* **2003**, *48*, 1531–1534.
95. Morris, W.; Doonan, C.J.; Furukawa, H.; Banerjee, R.; Yaghi, O.M. Crystals as molecules: Postsynthesis covalent functionalization of zeolitic imidazolate frameworks. *J. Am. Chem. Soc.* **2008**, *130*, 12626–12627. [CrossRef] [PubMed]
96. Wang, B.; Côté, A.P.; Furukawa, H.; O’Keeffe, M.; Yaghi, O.M. Colossal cages in zeolitic imidazolate frameworks as selective carbon dioxide reservoirs. *Nature* **2008**, *453*, 207–211. [CrossRef] [PubMed]
97. Jian, M.; Liu, B.; Liu, R.; Qu, J.; Wang, H.; Zhang, X. Water-based synthesis of zeolitic imidazolate framework-8 with high morphology level at room temperature. *RSC Adv.* **2015**, *5*, 48433–48441. [CrossRef]
98. Ethiraj, J.; Palla, S.; Reinsch, H. Insights into high pressure gas adsorption properties of ZIF-67: Experimental and theoretical studies. *Microporous Mesoporous Mater.* **2020**, *294*, 109867. [CrossRef]
99. Duan, C.; Yu, Y.; Yang, P.; Zhang, X.; Li, F.; Li, L.; Xi, H. Engineering new defects in MIL-100 (Fe) via a mixed-ligand approach to effect enhanced volatile organic compound adsorption capacity. *Ind. Eng. Chem. Res.* **2019**, *59*, 774–782. [CrossRef]
100. Duan, C.; Yu, Y.; Xiao, J.; Zhang, X.; Li, L.; Yang, P.; Wu, J.; Xi, H. Water-based routes for synthesis of metal–organic frameworks: A review. *Sci. China Mater.* **2020**, *63*, 667–685. [CrossRef]
101. Zhang, J.; Zhang, T.; Yu, D.; Xiao, K.; Hong, Y. Transition from ZIF-L-Co to ZIF-67: A new insight into the structural evolution of zeolitic imidazolate frameworks (ZIFs) in aqueous systems. *CrystEngComm* **2015**, *17*, 8212–8215. [CrossRef]
102. Bradshaw, D.; El-Hankari, S.; Lupica-Spagnolo, L.J.C.S.R. Supramolecular templating of hierarchically porous metal–organic frameworks. *Chem. Soc. Rev.* **2014**, *43*, 5431–5443. [CrossRef]
103. Duan, C.; Zhang, Y.; Li, J.; Kang, L.; Xie, Y.; Qiao, W.; Zhu, C.; Luo, H. Rapid room-temperature preparation of hierarchically porous metal–organic frameworks for efficient uranium removal from aqueous solutions. *Nanomaterials* **2020**, *10*, 1539. [CrossRef]
104. Sarawade, P.; Tan, H.; Polshettiwar, V. Shape- and morphology-controlled Sustainable synthesis of Cu, Co, and in metal organic frameworks with high CO₂ capture capacity. *ACS Sustain. Chem. Eng.* **2013**, *1*, 66–74. [CrossRef]
105. Hsu, S.-H.; Li, C.-T.; Chien, H.-T.; Salunkhe, R.R.; Suzuki, N.; Yamauchi, Y.; Ho, K.-C.; Wu, K.C.-W. Platinum-free counter electrode comprised of metal–organic-framework (MOF)-derived cobalt sulfide nanoparticles for efficient dye-sensitized solar cells (DSSCs). *Sci. Rep.* **2014**, *4*, 6983. [CrossRef] [PubMed]
106. Li, W.; Wang, K.; Yang, X.; Zhan, F.; Wang, Y.; Liu, M.; Qiu, X.; Li, J.; Zhan, J.; Li, Q. Surfactant-assisted controlled synthesis of a metal–organic framework on Fe₂O₃ nanorod for boosted photoelectrochemical water oxidation. *Chem. Eng. J.* **2020**, *379*, 122256. [CrossRef]
107. Sumida, K.; Liang, K.; Reboul, J.; Ibarra, I.A.; Furukawa, S.; Falcaro, P. Sol–gel processing of metal–organic frameworks. *Chem. Mater.* **2017**, *29*, 2626–2645. [CrossRef]
108. Marquez, A.G.; Horcajada, P.; Grosso, D.; Ferey, G.; Serre, C.; Sanchez, C.; Boissiere, C. Green scalable aerosol synthesis of porous metal–organic frameworks. *Chem. Commun.* **2013**, *49*, 3848–3850. [CrossRef]
109. Xu, L.; Xiong, Y.; Dang, B.; Ye, Z.; Jin, C.; Sun, Q.; Yu, X. In-situ anchoring of Fe₃O₄/ZIF-67 dodecahedrons in highly compressible wood aerogel with excellent microwave absorption properties. *Mater. Des.* **2019**, *182*, 108006. [CrossRef]
110. Chalati, T.; Horcajada, P.; Gref, R.; Couvreur, P.; Serre, C. Optimisation of the synthesis of MOF nanoparticles made of flexible porous iron fumarate MIL-88A. *J. Mater. Chem.* **2011**, *21*, 2220–2227. [CrossRef]
111. Babu, R.; Roshan, R.; Kathalikkattil, A.C.; Kim, D.W.; Park, D.-W. Rapid, microwave-assisted synthesis of cubic, three-dimensional, highly porous MOF-205 for room temperature CO₂ fixation via cyclic carbonate synthesis. *ACS Appl. Mater. Interfaces* **2016**, *8*, 33723–33731. [CrossRef]
112. Mahmoodi, N.M.; Taghizadeh, M.; Taghizadeh, A.; Abdi, J.; Hayati, B.; Shekarchi, A.A. Bio-based magnetic metal–organic framework nanocomposite: Ultrasound-assisted synthesis and pollutant (heavy metal and dye) removal from aqueous media. *Appl. Surf. Sci.* **2019**, *480*, 288–299. [CrossRef]
113. Sharsheeva, A.; Iglin, V.A.; Nesterov, P.V.; Kuchur, O.A.; Garifullina, E.; Hey-Hawkins, E.; Ulasevich, S.A.; Skorb, E.V.; Vinogradov, A.V.; Morozov, M.I. Light-controllable systems based on TiO₂-ZIF-8 composites for targeted drug release: Communicating with tumour cells. *J. Mater. Chem. B* **2019**, *7*, 6810–6821. [CrossRef]
114. Hwang, S.; Chi, W.S.; Lee, S.J.; Im, S.H.; Kim, J.H.; Kim, J. Hollow ZIF-8 nanoparticles improve the permeability of mixed matrix membranes for CO₂/CH₄ gas separation. *J. Membr. Sci.* **2015**, *480*, 11–19. [CrossRef]

115. Yang, Q.; Xu, Q.; Yu, S.H.; Jiang, H.L. Pd Nanocubes@ ZIF-8: Integration of Plasmon-Driven Photothermal Conversion with a Metal–Organic Framework for Efficient and Selective Catalysis. *Angew. Chem.* **2016**, *128*, 3749–3753. [[CrossRef](#)]
116. Yang, Y.; Wang, S.Q.; Wen, H.; Ye, T.; Chen, J.; Li, C.P.; Du, M. Nanoporous gold embedded ZIF composite for enhanced electrochemical nitrogen fixation. *Angew. Chem. Int. Ed.* **2019**, *58*, 15362–15366. [[CrossRef](#)] [[PubMed](#)]
117. Cai, G.; Ding, M.; Wu, Q.; Jiang, H.-L.J.N.s.r. Encapsulating soluble active species into hollow crystalline porous capsules beyond integration of homogeneous and heterogeneous catalysis. *Natl. Sci. Rev.* **2020**, *7*, 37–45. [[CrossRef](#)] [[PubMed](#)]
118. Dai, C.; Zhang, A.; Li, J.; Hou, K.; Liu, M.; Song, C.; Guo, X. Synthesis of yolk–shell HPW@ Hollow silicalite-1 for esterification reaction. *Chem. Commun.* **2014**, *50*, 4846–4848. [[CrossRef](#)] [[PubMed](#)]
119. Melgar, V.M.A.; Kim, J.; Othman, M.R. Zeolitic imidazolate framework membranes for gas separation: A review of synthesis methods and gas separation performance. *J. Ind. Eng. Chem.* **2015**, *28*, 1–15. [[CrossRef](#)]
120. Butler, K.T.; Worrall, S.D.; Molloy, C.D.; Hendon, C.H.; Atfield, M.P.; Dryfe, R.A.; Walsh, A.J.J.o.M.C.C. Electronic structure design for nanoporous, electrically conductive zeolitic imidazolate frameworks. *J. Mater. Chem. C* **2017**, *5*, 7726–7731. [[CrossRef](#)]
121. Lashgari, S.M.; Yari, H.; Mahdavian, M.; Ramezanzadeh, B.; Bahlakeh, G.; Ramezanzadeh, M. Application of nanoporous cobalt-based ZIF-67 metal-organic framework (MOF) for construction of an epoxy-composite coating with superior anti-corrosion properties. *Corros. Sci.* **2021**, *178*, 109099. [[CrossRef](#)]
122. Zhan, M.; Hussain, S.; AlGarni, T.S.; Shah, S.; Liu, J.; Zhang, X.; Ahmad, A.; Javed, M.S.; Qiao, G.; Liu, G. Facet controlled polyhedral ZIF-8 MOF nanostructures for excellent NO₂ gas-sensing applications. *Mater. Res. Bull.* **2021**, *136*, 111133. [[CrossRef](#)]
123. Wang, H.; Grabstanowicz, L.R.; Barkholtz, H.M.; Rebollar, D.; Kaiser, Z.B.; Zhao, D.; Chen, B.-H.; Liu, D.-J. Impacts of imidazolate ligand on performance of zeolitic-imidazolate framework-derived oxygen reduction catalysts. *ACS Energy Lett.* **2019**, *4*, 2500–2507. [[CrossRef](#)]
124. Kouser, S.; Hezam, A.; Khadri, M.; Khanum, S.A. A review on zeolite imidazole frameworks: Synthesis, properties, and applications. *J. Porous Mater.* **2022**, *29*, 663–681. [[CrossRef](#)]
125. Khan, S.; Cao, Q.; Zheng, Y.; Huang, Y.; Zhu, Y. Health risks of heavy metals in contaminated soils and food crops irrigated with wastewater in Beijing, China. *Environ. Pollut.* **2008**, *152*, 686–692. [[CrossRef](#)] [[PubMed](#)]
126. Huang, H.; Li, J.-R.; Wang, K.; Han, T.; Tong, M.; Li, L.; Xie, Y.; Yang, Q.; Liu, D.; Zhong, C. An in situ self-assembly template strategy for the preparation of hierarchical-pore metal-organic frameworks. *Nat. Commun.* **2015**, *6*, 8847. [[CrossRef](#)]
127. Qian, J.; Sun, F.; Qin, L. Hydrothermal synthesis of zeolitic imidazolate framework-67 (ZIF-67) nanocrystals. *Mater. Lett.* **2012**, *82*, 220–223. [[CrossRef](#)]
128. Wang, C.; Luan, J.; Wu, C. Metal-organic frameworks for aquatic arsenic removal. *Water Res.* **2019**, *158*, 370–382. [[CrossRef](#)] [[PubMed](#)]
129. Yao, J.; He, M.; Wang, H. Strategies for controlling crystal structure and reducing usage of organic ligand and solvents in the synthesis of zeolitic imidazolate frameworks. *CrystEngComm* **2015**, *17*, 4970–4976. [[CrossRef](#)]
130. Şahin, F.; Topuz, B.; Kalıpcılar, H. Synthesis of ZIF-7, ZIF-8, ZIF-67 and ZIF-L from recycled mother liquors. *Microporous Mesoporous Mater.* **2018**, *261*, 259–267. [[CrossRef](#)]
131. Demir, N.K.; Topuz, B.; Yilmaz, L.; Kalıpcılar, H. Synthesis of ZIF-8 from recycled mother liquors. *Microporous Mesoporous Mater.* **2014**, *198*, 291–300. [[CrossRef](#)]
132. Zhang, H.; Zhao, M.; Lin, Y. Stability of ZIF-8 in water under ambient conditions. *Microporous Mesoporous Mater.* **2019**, *279*, 201–210. [[CrossRef](#)]
133. Duke, M.C.; Zhu, B.; Doherty, C.M.; Hill, M.R.; Hill, A.J.; Carreon, M.A. Structural effects on SAPO-34 and ZIF-8 materials exposed to seawater solutions, and their potential as desalination membranes. *Desalination* **2016**, *377*, 128–137. [[CrossRef](#)]
134. Zhang, Y.; Xie, Z.; Wang, Z.; Feng, X.; Wang, Y.; Wu, A. Unveiling the adsorption mechanism of zeolitic imidazolate framework-8 with high efficiency for removal of copper ions from aqueous solutions. *Dalton Trans.* **2016**, *45*, 12653–12660. [[CrossRef](#)]
135. Liu, X.; Li, Y.; Ban, Y.; Peng, Y.; Jin, H.; Bux, H.; Xu, L.; Caro, J.; Yang, W. Improvement of hydrothermal stability of zeolitic imidazolate frameworks. *Chem. Commun.* **2013**, *49*, 9140–9142. [[CrossRef](#)] [[PubMed](#)]
136. Wang, H.; Jian, M.; Qi, Z.; Li, Y.; Liu, R.; Qu, J.; Zhang, X. Specific anion effects on the stability of zeolitic imidazolate framework-8 in aqueous solution. *Microporous Mesoporous Mater.* **2018**, *259*, 171–177. [[CrossRef](#)]
137. Ying, Y.; Pourrahimi, A.M.; Sofer, Z.K.; Matějková, S.; Pumera, M. Radioactive uranium preconcentration via self-propelled autonomous microrobots based on metal–organic frameworks. *ACS Nano* **2019**, *13*, 11477–11487. [[CrossRef](#)] [[PubMed](#)]
138. Zhang, T.; Zhang, X.; Yan, X.; Kong, L.; Zhang, G.; Liu, H.; Qiu, J.; Yeung, K.L. Synthesis of Fe₃O₄@ZIF-8 magnetic core–shell microspheres and their potential application in a capillary microreactor. *Chem. Eng. J.* **2013**, *228*, 398–404. [[CrossRef](#)]
139. Qiu, M.; He, C. Efficient removal of heavy metal ions by forward osmosis membrane with a polydopamine modified zeolitic imidazolate framework incorporated selective layer. *J. Hazard. Mater.* **2019**, *367*, 339–347. [[CrossRef](#)]
140. Nalaparaju, A.; Jiang, J. Ion exchange in metal–organic framework for water purification: Insight from molecular simulation. *J. Phys. Chem. C* **2012**, *116*, 6925–6931. [[CrossRef](#)]
141. Hou, X.; Zhou, H.; Zhang, J.; Cai, Y.; Huang, F.; Wei, Q. High Adsorption Pearl-Necklace-Like Composite Membrane Based on Metal–Organic Framework for Heavy Metal Ion Removal. *Part. Part. Syst. Charact.* **2018**, *35*, 1700438. [[CrossRef](#)]
142. Rowsell, J.L.; Yaghi, O.M. Effects of functionalization, catenation, and variation of the metal oxide and organic linking units on the low-pressure hydrogen adsorption properties of metal–organic frameworks. *J. Am. Chem. Soc.* **2006**, *128*, 1304–1315. [[CrossRef](#)]

143. Jacobs, P.; Flanigen, E.M.; Jansen, J.; van Bekkum, H. *Introduction to Zeolite Science and Practice*; Elsevier: Amsterdam, The Netherlands, 2001.
144. Yuan, X.; Wang, H.; Wang, J.; Zeng, G.; Chen, X.; Wu, Z.; Jiang, L.; Xiong, T.; Zhang, J.; Wang, H. Near-infrared-driven Cr (VI) reduction in aqueous solution based on a MoS₂/Sb₂S₃ photocatalyst. *Catal. Sci. Technol.* **2018**, *8*, 1545–1554. [[CrossRef](#)]
145. Jiang, L.; Yuan, X.; Zeng, G.; Liang, J.; Wu, Z.; Wang, H.; Zhang, J.; Xiong, T.; Li, H. A facile band alignment of polymeric carbon nitride isotype heterojunctions for enhanced photocatalytic tetracycline degradation. *Environ. Sci. Nano* **2018**, *5*, 2604–2617. [[CrossRef](#)]
146. Chen, X.; Mao, S.S. Titanium dioxide nanomaterials: Synthesis, properties, modifications, and applications. *Chem. Rev.* **2007**, *107*, 2891–2959. [[CrossRef](#)] [[PubMed](#)]
147. Fujishima, A.; Honda, K. Electrochemical photolysis of water at a semiconductor electrode. *Nature* **1972**, *238*, 37–38. [[CrossRef](#)] [[PubMed](#)]
148. Laurier, K.G.; Vermoortele, F.; Ameloot, R.; De Vos, D.E.; Hofkens, J.; Roeffaers, M.B. Iron (III)-based metal–organic frameworks as visible light photocatalysts. *J. Am. Chem. Soc.* **2013**, *135*, 14488–14491. [[CrossRef](#)] [[PubMed](#)]
149. Beni, F.A.; Gholami, A.; Ayati, A.; Shahrak, M.N.; Sillanpää, M.J.M.; Materials, M. UV-switchable phosphotungstic acid sandwiched between ZIF-8 and Au nanoparticles to improve simultaneous adsorption and UV light photocatalysis toward tetracycline degradation. *Microporous Mesoporous Mater.* **2020**, *303*, 110275. [[CrossRef](#)]
150. Park, H.; Reddy, D.A.; Kim, Y.; Ma, R.; Choi, J.; Kim, T.K.; Lee, K.-S. Zeolitic imidazolate framework-67 (ZIF-67) rhombic dodecahedrons as full-spectrum light harvesting photocatalyst for environmental remediation. *Solid State Sci.* **2016**, *62*, 82–89. [[CrossRef](#)]
151. Abbas, N.; Shao, G.N.; Haider, M.S.; Imran, S.; Park, S.S.; Kim, H.T. Sol–gel synthesis of TiO₂-Fe₂O₃ systems: Effects of Fe₂O₃ content and their photocatalytic properties. *J. Ind. Eng. Chem.* **2016**, *39*, 112–120. [[CrossRef](#)]
152. Han, F.; Kambala, V.; Dharmarajan, R.; Liu, Y.; Naidu, R. Photocatalytic degradation of azo dye acid orange 7 using different light sources over Fe³⁺-doped TiO₂ nanocatalysts. *Environ. Technol. Innov.* **2018**, *12*, 27–42. [[CrossRef](#)]
153. Mendiola-Alvarez, S.; Hernández-Ramírez, A.; Guzmán-Mar, J.; Maya-Treviño, M.; Caballero-Quintero, A.; Hinojosa-Reyes, L. A novel P-doped Fe₂O₃-TiO₂ mixed oxide: Synthesis, characterization and photocatalytic activity under visible radiation. *Catal. Today* **2019**, *328*, 91–98. [[CrossRef](#)]
154. Sharma, S.; Basu, S. Highly reusable visible light active hierarchical porous WO₃/SiO₂ monolith in centimeter length scale for enhanced photocatalytic degradation of toxic pollutants. *Sep. Purif. Technol.* **2020**, *231*, 115916. [[CrossRef](#)]
155. Zhou, J.; Liu, W.; Cai, W. The synergistic effect of Ag/AgCl@ ZIF-8 modified g-C₃N₄ composite and peroxymonosulfate for the enhanced visible-light photocatalytic degradation of levofloxacin. *Sci. Total Environ.* **2019**, *696*, 133962. [[CrossRef](#)]
156. Mahmoodi, N.M.; Keshavarzi, S.; Oveisi, M.; Rahimi, S.; Hayati, B. Metal-organic framework (ZIF-8)/inorganic nanofiber (Fe₂O₃) nanocomposite: Green synthesis and photocatalytic degradation using LED irradiation. *J. Mol. Liq.* **2019**, *291*, 111333. [[CrossRef](#)]
157. Ulrich, G.; Ziessel, R.; Harriman, A. The chemistry of fluorescent bodipy dyes: Versatility unsurpassed. *Angew. Chem. Int. Ed.* **2008**, *47*, 1184–1201. [[CrossRef](#)] [[PubMed](#)]
158. Loudet, A.; Burgess, K. BODIPY dyes and their derivatives: Syntheses and spectroscopic properties. *Chem. Rev.* **2007**, *107*, 4891–4932. [[CrossRef](#)] [[PubMed](#)]
159. Miensah, E.D.; Khan, M.M.; Chen, J.Y.; Zhang, X.M.; Wang, P.; Zhang, Z.X.; Jiao, Y.; Liu, Y.; Yang, Y. Zeolitic imidazolate frameworks and their derived materials for sequestration of radionuclides in the environment: A review. *Crit. Rev. Environ. Sci. Technol.* **2020**, *50*, 1874–1934. [[CrossRef](#)]
160. Wu, Z.; Yuan, X.; Zhong, H.; Wang, H.; Jiang, L.; Zeng, G.; Wang, H.; Liu, Z.; Li, Y. Highly efficient adsorption of Congo red in single and binary water with cationic dyes by reduced graphene oxide decorated NH₂-MIL-68 (Al). *J. Mol. Liq.* **2017**, *247*, 215–229. [[CrossRef](#)]
161. Xiong, T.; Yuan, X.; Wang, H.; Wu, Z.; Jiang, L.; Leng, L.; Xi, K.; Cao, X.; Zeng, G. Highly efficient removal of diclofenac sodium from medical wastewater by Mg/Al layered double hydroxide-poly (m-phenylenediamine) composite. *Chem. Eng. J.* **2019**, *366*, 83–91. [[CrossRef](#)]
162. Bahmani, E.; Koushkbaghi, S.; Darabi, M.; ZabihiSahebi, A.; Askari, A.; Irani, M. Fabrication of novel chitosan-g-PNVCL/ZIF-8 composite nanofibers for adsorption of Cr (VI), As (V) and phenol in a single and ternary systems. *Carbohydr. Polym.* **2019**, *224*, 115148. [[CrossRef](#)]
163. Wang, J.; Yu, S.; Feng, F.; Lu, L. Simultaneous purification and immobilization of laccase on magnetic zeolitic imidazolate frameworks: Recyclable biocatalysts with enhanced stability for dye decolorization. *Biochem. Eng. J.* **2019**, *150*, 107285. [[CrossRef](#)]
164. Dai, J.; Liu, Y.-X.; Xiao, S.-Z.; Liu, J.; He, J.; Lei, J.-D.; Wang, L.-Y. The ZIF-8 Based on Poly Microspheres as A Novel Adsorbent for Removing Organic Contaminants from Wastewater. Proceedings of 3rd 2017 International Conference on Sustainable Development (ICSD 2017), New York, NY, USA, 18–20 September 2017; pp. 118–124.
165. Nematollahzadeh, A.; Babapoor, A.; Mousavi, S.M.; Nuri, A. Nitrobenzene adsorption from aqueous solution onto polythiophene-modified magnetite nanoparticles. *Mater. Chem. Phys.* **2021**, *262*, 124266. [[CrossRef](#)]
166. Sharma, B.; Dangi, A.K.; Shukla, P. Contemporary enzyme based technologies for bioremediation: A review. *J. Environ. Manag.* **2018**, *210*, 10–22. [[CrossRef](#)]
167. Zhao, R.; Wang, Y.; Li, X.; Sun, B.; Wang, C. Synthesis of β -cyclodextrin-based electrospun nanofiber membranes for highly efficient adsorption and separation of methylene blue. *ACS Appl. Mater. Interfaces* **2015**, *7*, 26649–26657. [[CrossRef](#)] [[PubMed](#)]

168. Mousavi, M.; Hashemi, A.; Arjmand, O.; Amani, A.M.; Babapoor, A.; Fateh, M.A.; Fateh, H.; Mojoudi, F.; Esmaeili, H.; Jahandideh, S. Erythrosine adsorption from aqueous solution via decorated graphene oxide with magnetic iron oxide nano particles: Kinetic and equilibrium studies. *Acta Chim. Slov.* **2018**, *65*, 882–894. [[CrossRef](#)] [[PubMed](#)]
169. Zahra, R.; Pervaiz, E.; Yang, M.; Rabi, O.; Saleem, Z.; Ali, M.; Farrukh, S. A review on nickel cobalt sulphide and their hybrids: Earth abundant, pH stable electro-catalyst for hydrogen evolution reaction. *Int. J. Hydrogen Energy* **2020**, *45*, 24518–24543. [[CrossRef](#)]
170. Yang, D.; Yuan, Y.; Wang, L.; Wang, X.; Mu, R.; Pang, J.; Xiao, J.; Zheng, Y. A review on konjac glucomannan gels: Microstructure and application. *Int. J. Mol. Sci.* **2017**, *18*, 2250. [[CrossRef](#)] [[PubMed](#)]
171. Li, S.; Zhang, X.; Huang, Y. Zeolitic imidazolate framework-8 derived nanoporous carbon as an effective and recyclable adsorbent for removal of ciprofloxacin antibiotics from water. *J. Hazard. Mater.* **2017**, *321*, 711–719. [[CrossRef](#)] [[PubMed](#)]
172. Li, N.; Zhou, L.; Jin, X.; Owens, G.; Chen, Z. Simultaneous removal of tetracycline and oxytetracycline antibiotics from wastewater using a ZIF-8 metal organic-framework. *J. Hazard. Mater.* **2019**, *366*, 563–572. [[CrossRef](#)]
173. Ahmadi, S.; Kalaei, M.; Moradi, O.; Nosratinia, F.; Abdouss, M. Synthesis of novel zeolitic imidazolate framework (ZIF-67)–zinc oxide (ZnO) nanocomposite (ZnO@ZIF-67) and potential adsorption of pharmaceutical (tetracycline (TCC)) from water. *J. Mol. Struct.* **2022**, *1251*, 132013. [[CrossRef](#)]
174. Chen, G.; He, S.; Shi, G.; Ma, Y.; Ruan, C.; Jin, X.; Chen, Q.; Liu, X.; Dai, H.; Chen, X. In-situ immobilization of ZIF-67 on wood aerogel for effective removal of tetracycline from water. *Chem. Eng. J.* **2021**, *423*, 130184. [[CrossRef](#)]
175. Lyu, J.; Zhang, N.; Liu, H.; Zeng, Z.; Zhang, J.; Bai, P.; Guo, X. Adsorptive removal of boron by zeolitic imidazolate framework: Kinetics, isotherms, thermodynamics, mechanism and recycling. *Sep. Purif. Technol.* **2017**, *187*, 67–75. [[CrossRef](#)]
176. de Souza, E.C.; Pimenta, A.S.; da Silva, A.J.F.; do Nascimento, P.F.P.; Ighalo, J.O. Oxidized eucalyptus charcoal: A renewable biosorbent for removing heavy metals from aqueous solutions. *Biomass Convers. Biorefinery* **2021**, 1–15. [[CrossRef](#)]
177. Van Tran, T.; Nguyen, H.; Le, P.H.A.; Nguyen, D.T.C.; Nguyen, T.T.; Van Nguyen, C.; Vo, D.-V.N.; Nguyen, T.D. Microwave-assisted solvothermal fabrication of hybrid zeolitic–imidazolate framework (ZIF-8) for optimizing dyes adsorption efficiency using response surface methodology. *J. Environ. Chem. Eng.* **2020**, *8*, 104189. [[CrossRef](#)]
178. Jiang, C.; Fu, B.; Cai, H.; Cai, T. Efficient adsorptive removal of Congo red from aqueous solution by synthesized zeolitic imidazolate framework-8. *Chem. Speciat. Bioavailab.* **2016**, *28*, 199–208. [[CrossRef](#)]
179. Igwegbe, C.A.; Onukwuli, O.D.; Ighalo, J.O.; Okoye, P.U. Adsorption of cationic dyes on Dacryodes edulis seeds activated carbon modified using phosphoric acid and sodium chloride. *Environ. Process.* **2020**, *7*, 1151–1171. [[CrossRef](#)]
180. Abdi, J.; Vossoughi, M.; Mahmoodi, N.M.; Alemzadeh, I. Synthesis of amine-modified zeolitic imidazolate framework-8, ultrasound-assisted dye removal and modeling. *Ultrason. Sonochem.* **2017**, *39*, 550–564. [[CrossRef](#)]
181. Kulkarni, S.; Dhokpande, S.; Kaware, J. A review on isotherms and kinetics of heavy metal removal. *Int. J. Ethics Eng. Manag. Educ.* **2014**, *1*, 1–4.
182. Pan, Y.; Li, Z.; Zhang, Z.; Tong, X.-S.; Li, H.; Jia, C.-Z.; Liu, B.; Sun, C.-Y.; Yang, L.-Y.; Chen, G.-J. Adsorptive removal of phenol from aqueous solution with zeolitic imidazolate framework-67. *J. Environ. Manag.* **2016**, *169*, 167–173. [[CrossRef](#)]
183. Su, S.; Che, R.; Liu, Q.; Liu, J.; Zhang, H.; Li, R.; Jing, X.; Wang, J. Zeolitic Imidazolate Framework-67: A promising candidate for recovery of uranium (VI) from seawater. *Colloids Surf. A Physicochem. Eng. Asp.* **2018**, *547*, 73–80. [[CrossRef](#)]
184. Feng, Y.; Li, Y.; Xu, M.; Liu, S.; Yao, J. Fast adsorption of methyl blue on zeolitic imidazolate framework-8 and its adsorption mechanism. *RSC Adv.* **2016**, *6*, 109608–109612. [[CrossRef](#)]
185. Pillai, P.; Dharaskar, S.; Sasikumar, S.; Khalid, M. Zeolitic imidazolate framework-8 nanoparticle: A promising adsorbent for effective fluoride removal from aqueous solution. *Appl. Water Sci.* **2019**, *9*, 150. [[CrossRef](#)]
186. Shams, M.; Dehghani, M.H.; Nabizadeh, R.; Mesdaghinia, A.; Alimohammadi, M.; Najafpoor, A.A. Adsorption of phosphorus from aqueous solution by cubic zeolitic imidazolate framework-8: Modeling, mechanical agitation versus sonication. *J. Mol. Liq.* **2016**, *224*, 151–157. [[CrossRef](#)]
187. Fan, C.; Liang, Y.; Dong, H.; Yang, J.; Tang, G.; Zhang, W.; Kong, D.; Li, J.; Cao, Y. Guanidinium ionic liquid-controlled synthesis of zeolitic imidazolate framework for improving its adsorption property. *Sci. Total Environ.* **2018**, *640*, 163–173. [[CrossRef](#)] [[PubMed](#)]
188. Kim, M.I.; Kim, S.; Kim, T.; Lee, D.K.; Seo, B.; Lim, C.-S. Mechanical and thermal properties of epoxy composites containing zirconium oxide impregnated halloysite nanotubes. *Coatings* **2017**, *7*, 231. [[CrossRef](#)]
189. Tran, H.N.; You, S.-J.; Hosseini-Bandegharaei, A.; Chao, H.-P. Mistakes and inconsistencies regarding adsorption of contaminants from aqueous solutions: A critical review. *Water Res.* **2017**, *120*, 88–116. [[CrossRef](#)] [[PubMed](#)]
190. Igwegbe, C.A.; Oba, S.N.; Aniagor, C.O.; Adeniyi, A.G.; Ighalo, J.O. Adsorption of ciprofloxacin from water: A comprehensive review. *J. Ind. Eng. Chem.* **2021**, *93*, 57–77. [[CrossRef](#)]
191. Nasir, A.M.; Nordin, N.M.; Goh, P.; Ismail, A. Application of two-dimensional leaf-shaped zeolitic imidazolate framework (2D ZIF-L) as arsenite adsorbent: Kinetic, isotherm and mechanism. *J. Mol. Liq.* **2018**, *250*, 269–277. [[CrossRef](#)]
192. Yan, X.; Hu, X.; Chen, T.; Zhang, S.; Zhou, M. Adsorptive removal of 1-naphthol from water with Zeolitic imidazolate framework-67. *J. Phys. Chem. Solids* **2017**, *107*, 50–54. [[CrossRef](#)]
193. Tu, N.T.T.; Thien, T.V.; Du, P.D.; Chau, V.T.T.; Mau, T.X.; Khieu, D.Q. Adsorptive removal of Congo red from aqueous solution using zeolitic imidazolate framework-67. *J. Environ. Chem. Eng.* **2018**, *6*, 2269–2280.

194. Moghaddam, M.H.; Nabizadeh, R.; Dehghani, M.H.; Akbarpour, B.; Azari, A.; Yousefi, M. Performance investigation of Zeolitic Imidazolate framework-8 (ZIF-8) in the removal of trichloroethylene from aqueous solutions. *Microchem. J.* **2019**, *150*, 104185. [[CrossRef](#)]
195. Lin, K.-Y.A.; Yang, H.; Lee, W.-D. Enhanced removal of diclofenac from water using a zeolitic imidazole framework functionalized with cetyltrimethylammonium bromide (CTAB). *RSC Adv.* **2015**, *5*, 81330–81340.
196. Zhan, Y.; Guan, X.; Ren, E.; Lin, S.; Lan, J. Fabrication of zeolitic imidazolate framework-8 functional polyacrylonitrile nanofibrous mats for dye removal. *J. Polym. Res.* **2019**, *26*, 145. [[CrossRef](#)]
197. Liang, C.; Zhang, X.; Feng, P.; Chai, H.; Huang, Y. ZIF-67 derived hollow cobalt sulfide as superior adsorbent for effective adsorption removal of ciprofloxacin antibiotics. *Chem. Eng. J.* **2018**, *344*, 95–104. [[CrossRef](#)]
198. Liu, J.; Li, R.; Wang, Y.; Wang, Y.; Zhang, X.; Fan, C. The active roles of ZIF-8 on the enhanced visible photocatalytic activity of Ag/AgCl: Generation of superoxide radical and adsorption. *J. Alloys Compd.* **2017**, *693*, 543–549. [[CrossRef](#)]
199. Fan, G.; Zheng, X.; Luo, J.; Peng, H.; Lin, H.; Bao, M.; Hong, L.; Zhou, J. Rapid synthesis of Ag/AgCl@ZIF-8 as a highly efficient photocatalyst for degradation of acetaminophen under visible light. *Chem. Eng. J.* **2018**, *351*, 782–790. [[CrossRef](#)]
200. Fan, G.; Luo, J.; Guo, L.; Lin, R.; Zheng, X.; Snyder, S.A. Doping Ag/AgCl in zeolitic imidazolate framework-8 (ZIF-8) to enhance the performance of photodegradation of methylene blue. *Chemosphere* **2018**, *209*, 44–52. [[CrossRef](#)] [[PubMed](#)]
201. Shi, F.; Chen, L.; Chen, M.; Jiang, D. Ag₃C₃N₄/nanocarbon/ZnIn₂S₄ nanocomposite: An artificial Z-scheme visible-light photocatalytic system using nanocarbon as the electron mediator. *Chem. Commun.* **2015**, *51*, 17144–17147. [[CrossRef](#)]
202. Ye, L.; Liu, J.; Gong, C.; Tian, L.; Peng, T.; Zan, L. Two different roles of metallic Ag on Ag/AgX/BiOX (X= Cl, Br) visible light photocatalysts: Surface plasmon resonance and Z-scheme bridge. *ACS Catal.* **2012**, *2*, 1677–1683. [[CrossRef](#)]
203. Liu, J.; Li, R.; Hu, Y.; Li, T.; Jia, Z.; Wang, Y.; Wang, Y.; Zhang, X.; Fan, C. Harnessing Ag nanofilm as an electrons transfer mediator for enhanced visible light photocatalytic performance of Ag@AgCl/Ag nanofilm/ZIF-8 photocatalyst. *Appl. Catal. B Environ.* **2017**, *202*, 64–71. [[CrossRef](#)]
204. Rohani, S.; Isimjan, T.; Mohamed, A.; Kazemian, H.; Salem, M.; Wang, T. Fabrication, modification and environmental applications of TiO₂ nanotube arrays (TNTAs) and nanoparticles. *Front. Chem. Sci. Eng.* **2012**, *6*, 112–122. [[CrossRef](#)]
205. Hu, C.; Xu, W.; Mo, X.; Li, H.; Zhou, S.; Zhang, P.; Tang, K. Efficient adsorption toward precious metal from aqueous solution by zeolitic imidazolate framework-8. *Adsorption* **2018**, *24*, 733–744. [[CrossRef](#)]
206. Wang, X.; Liu, J.; Leong, S.; Lin, X.; Wei, J.; Kong, B.; Xu, Y.; Low, Z.-X.; Yao, J.; Wang, H. Rapid construction of ZnO@ZIF-8 heterostructures with size-selective photocatalysis properties. *ACS Appl. Mater. Interfaces* **2016**, *8*, 9080–9087. [[CrossRef](#)]
207. Bethi, B.; Radhika, G.B.; Thang, L.M.; Sonawane, S.H.; Boczkaj, G.J.E.S.; Research, P. Photocatalytic decolourization of Rhodamine-B dye by visible light active ZIF-8/BiFeO₃ composite. *Environ. Sci. Pollut. Res.* **2022**, *1*–14. [[CrossRef](#)] [[PubMed](#)]
208. Li, R.; Li, W.; Jin, C.; He, Q.; Wang, Y. Fabrication of ZIF-8@TiO₂ micron composite via hydrothermal method with enhanced absorption and photocatalytic activities in tetracycline degradation. *J. Alloys Compd.* **2020**, *825*, 154008. [[CrossRef](#)]
209. Guan, W.; Gao, X.; Ji, G.; Xing, Y.; Du, C.; Liu, Z. Fabrication of a magnetic nanocomposite photocatalysts Fe₃O₄@ZIF-67 for degradation of dyes in water under visible light irradiation. *J. Solid State Chem.* **2017**, *255*, 150–156. [[CrossRef](#)]
210. Flihh, S.M.; Ammar, S.H. Fabrication and photocatalytic degradation activity of core/shell ZIF-67@CoWO₄@CoS heterostructure photocatalysts under visible light. *Environ. Nanotechnol. Monit. Manag.* **2021**, *16*, 100595. [[CrossRef](#)]
211. Chen, W.-Q.; Li, L.-Y.; Li, L.; Qiu, W.-H.; Tang, L.; Xu, L.; Xu, K.-J.; Wu, M.-H. MoS₂/ZIF-8 hybrid materials for environmental catalysis: Solar-driven antibiotic-degradation engineering. *Engineering* **2019**, *5*, 755–767. [[CrossRef](#)]
212. Guo, X.; He, S.; Meng, Z.; Wang, Y.; Peng, Y. Ag@ZIF-8/gC₃N₄Z-scheme photocatalyst for the enhanced removal of multiple classes of antibiotics by integrated adsorption and photocatalytic degradation under visible light irradiation. *RSC Adv.* **2022**, *12*, 17919–17931. [[CrossRef](#)]
213. Askari, N.; Beheshti, M.; Mowla, D.; Farhadian, M. Fabrication of CuWO₄/Bi₂S₃/ZIF₆₇ MOF: A novel double Z-scheme ternary heterostructure for boosting visible-light photodegradation of antibiotics. *Chemosphere* **2020**, *251*, 126453. [[CrossRef](#)]
214. Hou, W.; Huang, Y.; Liu, X. Highly efficient and recyclable ZIF-67 catalyst for the degradation of tetracycline. *Catal. Lett.* **2020**, *150*, 3017–3022. [[CrossRef](#)]
215. Ighalo, J.O.; Ajala, O.J.; Umenweke, G.; Ogunniyi, S.; Adeyanju, C.A.; Igwegbe, C.A.; Adeniyi, A.G. Mitigation of clofibrac acid pollution by adsorption: A review of recent developments. *J. Environ. Chem. Eng.* **2020**, *8*, 104264. [[CrossRef](#)]
216. Hevira, L.; Ighalo, J.O.; Aziz, H.; Zein, R. Terminalia catappa shell as low-cost biosorbent for the removal of methylene blue from aqueous solutions. *J. Ind. Eng. Chem.* **2021**, *97*, 188–199. [[CrossRef](#)]
217. Panda, J.; Sahoo, J.K.; Panda, P.K.; Sahu, S.N.; Samal, M.; Pattanayak, S.K.; Sahu, R. Adsorptive behavior of zeolitic imidazolate framework-8 towards anionic dye in aqueous media: Combined experimental and molecular docking study. *J. Mol. Liq.* **2019**, *278*, 536–545. [[CrossRef](#)]
218. Seo, P.W.; Song, J.Y.; Jhung, S.H. Adsorptive removal of hazardous organics from water with metal-organic frameworks. *Appl. Chem. Eng.* **2016**, *27*, 358–365. [[CrossRef](#)]
219. Lin, K.-Y.A.; Lee, W.-D. Highly efficient removal of Malachite green from water by a magnetic reduced graphene oxide/zeolitic imidazolate framework self-assembled nanocomposite. *Appl. Surf. Sci.* **2016**, *361*, 114–121. [[CrossRef](#)]
220. Li, X.; Gao, X.; Ai, L.; Jiang, J. Mechanistic insight into the interaction and adsorption of Cr (VI) with zeolitic imidazolate framework-67 microcrystals from aqueous solution. *Chem. Eng. J.* **2015**, *274*, 238–246. [[CrossRef](#)]

221. Khan, N.A.; Jung, B.K.; Hasan, Z.; Jhung, S.H. Adsorption and removal of phthalic acid and diethyl phthalate from water with zeolitic imidazolate and metal–organic frameworks. *J. Hazard. Mater.* **2015**, *282*, 194–200. [[CrossRef](#)]
222. Jung, B.K.; Jun, J.W.; Hasan, Z.; Jhung, S.H. Adsorptive removal of p-arsanilic acid from water using mesoporous zeolitic imidazolate framework-8. *Chem. Eng. J.* **2015**, *267*, 9–15. [[CrossRef](#)]
223. Ighalo, J.O.; Rangabhashiyam, S.; Adeyanju, C.A.; Ogunniyi, S.; Adeniyi, A.G.; Igwegbe, C.A. Zeolitic imidazolate frameworks (ZIFs) for aqueous phase adsorption—A review. *J. Ind. Eng. Chem.* **2022**, *105*, 34–48. [[CrossRef](#)]

Disclaimer/Publisher’s Note: The statements, opinions and data contained in all publications are solely those of the individual author(s) and contributor(s) and not of MDPI and/or the editor(s). MDPI and/or the editor(s) disclaim responsibility for any injury to people or property resulting from any ideas, methods, instructions or products referred to in the content.